Volume Change of the Tasman Glacier using Remote Sensing

A thesis submitted in fulfillment
of the requirements for the degree of
Master of Science in Geography at the
University of Canterbury

Written and prepared by Joel Thomas
Compiled April 3, 2009

Abstract

Mountain glaciers are expected to be the greatest contributor to sea level rise over the next century. Glaciers provide a good indicator of global climate and how to monitor their change is an increasingly important issue for climate science and for sea level rise forecasts. However, there has been little direct measurement of glacier volume change in New Zealand.

This study explores the use of remotely sensed data for measuring glacier volume change from 1965 to 2006. Digital photogrammetric methods were used to extract topographic data of the Tasman Glacier from aerial photography and ASTER imagery for the years 1965, 1986, 2002 and 2006. SRTM C band data from 2000 were also analysed.

Data were compared to an existing digital elvation model produced from the New Zealand Digital Topographic Database to test for their reliability. Using regression analysis, the data were filtered and points representing rock were used to correct points on the glacier ice for vertical bias.

The quality of the data extracted from the aerial photography was good on rock and debris covered ice, but poor on snow. The data extracted from ASTER was much more reliable on snow in the upper glacier than the aerial photography, but was very poor in the lower debris covered region of the glacier. While the quality of the SRTM data is very high, there is a second order distortion present in the data that is evident over elevation differences. However, the overall mean difference of the SRTM rock from TOPODATA is close to zero.

An overall trend could be seen in the data between dates. However, the 2006 ASTER data proved unreliable on the debris covered section of the glacier. Total volume change is therefore calculated for the period between 1965 and 2002. The data show a loss of 3.4 km^3 or 0.092 km^3 per year, an estimated 6% of the total ice in New Zealand. This is compared to estimates using the annual end of summer snowline survey between 1977 and 2005 of 1.78 km^3, or 0.064km^3 per year.

The spatial resolution of ASTER makes high temporal resolution monitoring of volume change unlikely for the New Zealand glaciers. The infrequency of aerial photography, the high cost and vast time involved in extracting good quality elevation data from aerial photography makes it impractical for monitoring glacier volume change remotely. However, SRTM and other radar sensors may provide a better solution, as the data do not rely heavily on user processing.

Acknowledgements

Lady Isaac and the Sir Neil Isaac Trust supported me finacially for the duration of this study, which is greatly appreciated. Without the Isaac Scholarship I would not have been able to carry on as a student and may never have completed this work.

Thanks a lot to Wendy Lawson and Wolfgang Rack for their help, encouragement and support as my supervisors. I have also had help from many other people at various stages of my thesis. Bob Williams from Marsterton High School for his help surveying the Tasman profiles (or perhaps it was the other way around). Rhys Gardiner for his help collecting GCPs. Andrew Willsman from NIWA for letting me in on his helicopter adventure up the Tasman and Murchison Glaciers. Trevor Chinn for putting up with me ferriting through his maps and photographs for several days. Brian Grant from the school of surveying at Otago, who I have only ever communicated with by email, for scanning the aerial photographs for me. Tim Kerr and Simon Allen for their help and discussions throughout the course of this work. And to Angelique for everything.

Contents

List of Figures

List of Tables

Chapter 1

Introduction

1.1 Mountain Glaciers, Climate and Sea Level Change

Changing mountain glaciers are the clearest visible evidence for climate change and are expected to contribute around 60% of the total eustatic sea level rise over the next century (Meier et al., 2007). In global context, New Zealand glaciers make up a fraction of the estimated total ice volume. Of all the land based ice on Earth, $\sim 96\%$ is locked up in the two ice sheets of Antarctica and Greenland. The rest is distributed around the Earth in the smaller mountain glaciers and ice caps (Meier and Bahr, 1996). The New Zealand glaciers make up about 1 percent of this total, 0.01% of the total ice mass world wide (Fitzharris et al., 1999). However, although this a relatively small amount of ice, it is significant for the Southern Hemisphere as it represents about one fifth of its mountain glacier ice. The New Zealand glaciers are also the most well studied in the Southern Hemisphere, providing valuable information for global climate models and reconstructions of climate histories. The maritime climate and steep topography of New Zealand means its glaciers are highly sensitive to climate perturbations.

There have been various estimations of the amount of sea level rise caused by melting mountain glaciers. Meier (1984) calculated that the amount of sea level rise observed from 1884 to 1975 that could be attributed to melting mountain glaciers was approximately one third of the total rise. This rise was about equal to what Gornitz et al. (1982) could not explain by thermal expansion of the sea. The estimates have been refined on an ongoing basis. Meier et al. (2003) estimated that mountain glaciers contributed 0.3 mm yr^{-1} sea level rise from 1961 to 1988 and that rate was thought to have increased to about 0.5 mm yr^{-1} since 1988. Meier et al. (2007) now estimate that the melting is accelerating and is now contributing 1.1 ± 0.24 mm yr^{-1}.

The best current estimate of total sea level change over the last century, based mostly on tide gauges, is 1.5 ± 0.5 mm yr^{-1}. However, independent estimates of the individual contributions to sea level change are much more uncertain, and when summed, suggest a total sea level rise of 0.7 ± 1.5 mm yr^{-1} (Cazenave and Nerem, 2004).

It is clear that these analyses have a high degree of uncertainty associated with the resulting

estimates. In particular, the data used to calculate the contribution of the New Zealand glaciers over this time period are based on limited mass balance measurements of the Tasman and Ivory Glaciers in the 1960s and 70s, and estimates derived from data collected in the Northern Hemisphere (Dyurgerov and Meier, 1997). Whether or not this is a suitable method is unknown as there is little data to test it against. The most complete mass balance record for a glacier in New Zealand is for the Ivory Glacier, where data were collected continuously for seven years from 1969 to 1975. The end of summer snowline (EOSS) survey, which began in 1977, provides a long term proxy for the mass balance of 46 index glaciers across the South Island (Chinn, 1995). However, these data sets do not provide direct quantitative information of glacier volume change and their contribution to sea level rise.

Glaciers and ice sheets have a direct but complex relationship with the climate system containing several feedback mechanisms. The exchange of water as a result of this relationship causes fluctuations in sea level (Figure 1.1). The general regional climate and local topography produce the local glacier climate through orographic and other local climate effects. The climate affects the net mass balance of a glacier by producing spatial variations of precipitation and temperature. Temperature and radiation determine the glacier's energy budget; if there is a surplus of energy, the ice warms and melting can occur. Temperate glaciers are particularly sensitive to changing energy budgets as they are close to or at the melting point.

Melting or accumulation causes the glacier to respond geometrically, gaining or losing volume and changing the local topography. The amount of runoff from the glacier is affected and therefore the amount of water that reaches the sea may change. The geometric response of a glacier can be used to assess the change in glacier volume and is key to this study.

Glaciers provide some of the best evidence for Quaternary climate variations. Past climatic conditions may be reconstructed without the need for instrumental climate records, based on proxy indicators in the modified landscapes that are left behind by glacial systems. For example, terminal moraines give clear evidence for past extent of glacier ice, while lateral moraines and trim lines show past thickness. Since 1874, instrumental mass balance measurements have been carried out on some glaciers around the world, mostly in the European Alps (Dyurgerov and Meier, 1997). This period approximately coincides with the end of the Little Ice Age (LIA), a worldwide cold period beginning in the thirteenth and fourteenth centuries (Grove, 2004). This means that virtually all instrumental records of glacier change worldwide have shown dramatic recession (Barry, 2006).

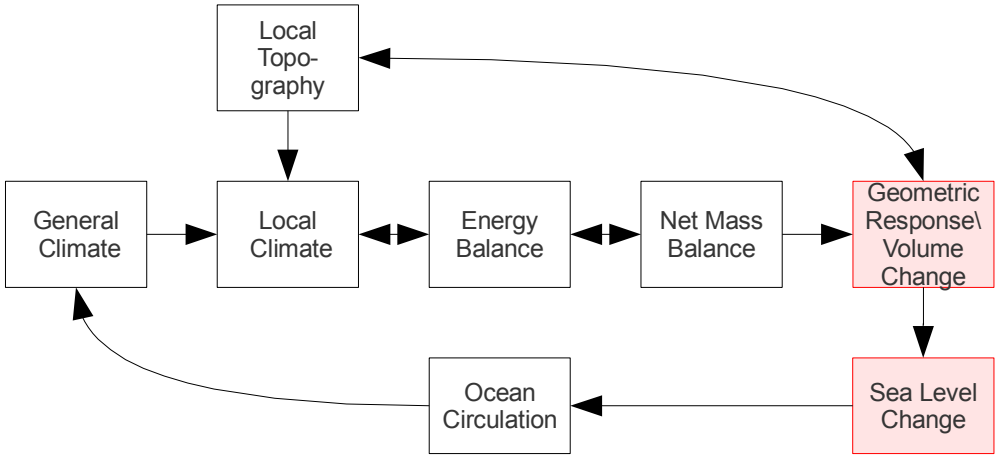

Figure 1.1: Glacier response and interaction with climate change. This study focuses on the the geometric response/volume change and sea level change components of the model. Modified from Meier (1965); Paterson (1994); Andrews (2006).

1.2 Detecting Glacier Volume Change

Volume change of glaciers occurs as a result of change in mass balance. Detecting volume change as well as measuring mass balance are key methods for monitoring the impacts of climate on the cryosphere.

Positive net mass balance indicates increased glacier volume. The glacier will respond to this by changing its shape, which is usually first observed as an advancing terminus position or increased thickness in the ablation zone. Conversely, the opposite will occur if the balance is negative (Paterson, 1994; Hooke, 2005). The net mass balance of a glacier in the mid latitudes can be defined as the sum of winter accumulation of mass plus the summer ablation (loss):

$$b_n = b_w + b_s \tag{1.1}$$

where b_n is the net mass balance for a balance year, b_w is the winter accumulation and b_s is the summer ablation. b_n is usually normalised by the area of the glacier. The overall health of the glacier can be evaluated from:

$$b_n = \int_A (b_w + b_s) dA \tag{1.2}$$

where A is the area of the glacier and b_n is the total net balance (Hooke, 2005).

The components of Equations 1.1 and 1.2 are determined by measuring surface elevation changes across the glacier in regular elevation bands, which are then integrated across the area of the whole glacier.

1.2.1 Glaciological Methods

The most common way to measure mass balance is to use a series of stakes placed within each elevation band in the ablation zone and regularly measuring the level of ice relative to the stakes. Holes must be drilled into the ice for the stakes to be placed into and their precise location and elevation determined. Measuring accumulation usually requires digging a series of pits in the accumulation zone to find a previously measured snow horizon (Østrem and Brugman, 1991). This may significantly underestimate actual volume loss because it usually does not take into account calving from the terminal face (Dyurgerov, 2003), which for many of the large valley glaciers in New Zealand may be significant. The high costs and labourious nature of frequent re-drilling and measuring of stakes means that only around 300 glaciers worldwide have been measured in this way, of which only around 40 have been measured regularly for 20 years or more (Dyurgerov and Meier, 1997). This method results in a significant amount of interpolating between points, meaning that although the general health of the glacier may be reasonably determined, actual volume change and water equivalent may be unrepresentative. However, it is still the most common method for monitoring individual glaciers and can provide detailed information regarding the spatial variation of ice volume change.

1.2.2 Geodetic Methods

Geodetic methods involve measuring the change in surface elevation over the entire glacier with respect to some reference datum. This can be done using differential GPS. However, this also suffers from similar costs and logistical problems as the glaciological method.

Recent work has demonstrated the ability to monitor the changing volume of mountain glacier systems using remote sensing to determine their contribution to sea level rise. Remote sensing can be used to produce digital elevation models (DEMs) of the glacier surface without the necessity for field work. The advantage is that the net mass balance may be determined for a whole set or system of glaciers at the same time and provide an overall change in volume for a certain time period. However, the separate components of Equations 1.1 and 1.2 may not so easily be determined. Hubbard et al. (2000) have shown that a combination of the two methods may produce the best results for identifying links with climate patterns.

Sapiano et al. (1998) used an infrared elevation profiling system on board a light aircraft to compare the surface elevation of nine North American glaciers to 1:10,000 scale topographic map contours produced by photogrammetric methods in late 1950s.

A similar approach was used by Arendt et al. (2002), who measured the volume change of 67 Alaskan glaciers from the mid 1950s to the mid 1990s. DEMs derived from airborne laser altimetry were compared with contours from 15 min USGS topographic maps. Although this method proved to be highly effective at measuring glacier volume change, airborne remote sensing is expensive and irregular.

Rignot et al. (2003) compared data from the Shuttle Radar Topography Mission (SRTM) to DEMs produced from topographic maps that were compiled from 1968 to 1975 for 63 large glaciers in Patagonia. The study was later extended to produce more detailed data of the glaciers within

the Torres del Paine National Park in Southern Patagonia using ASTER and Landsat ETM+ satellite imagery as well as aerial photography (Rivera and Casassa, 2004). The use of these data and methods was shown to be ideal due to the low costs and logistical requirements.

Numerous studies have focused on measuring volume change of a small number of glaciers with particular focus on the methodological processes rather than results. Vignon et al. (2003) used SRTM, ASTER and topographic maps to produce DEMs of three small glaciers ranging from 2.3 to 0.7 km^2 in extent in Peru. However, the RMS errors were estimated to be about the same as the estimated change. Berthier et al. (2004) effectively overcame the problem of large RMS errors by averaging the pixel values over 50 metre elevation bands. This method was applied to the Mer de Glace using DEMs derived from aerial photography and SPOT satellite imagery, achieving an estimated vertical error of one metre.

Berthier et al. (2006) assessed the accuracy of SRTM data for volume change estimates and found that at high altitudes, elevation was biased by up to -10 m. This puts into question previous attempts to use the SRTM data for measuring volume change; where SRTM was used as the most recent data set, significant overestimation of the volume change may have occurred.

Van Looy et al. (2006) also discovered an elevation bias with the SRTM data, after comparing it to a flat area of a USGS DEM for the Kenai Peninsula, Alaska. They found that the bias was not uniform, being greater over steeper terrain. For this reason steep areas such as nunataks were masked from the analysis. Although some good results were assumed for the ablation zones, caution was taken in drawing any conclusions for the accumulation zones due to the theoretical C-band penetration of dry snow (Ulaby et al., 1986; Rignot et al., 2001).

1.3 Monitoring Glacier Change

There are several worldwide glacier monitoring programmes, to which New Zealand has made limited and irregular contributions. The World Glacier Monitoring Service (WGMS) has published the Fluctuations of Glaciers (FOG) report about every five years since 1967 (IUGG et al., 2005). These reports contain a compilation of measurements such as frontal position, mass balance, changes in area, volume and thickness for glaciers world wide based on fairly standardised data from many sources. These reports have shown a steady decline of glacier mass over much of the Earth.

Dyurgerov (2002) compiled and summarised mass balance data from the WGMS data set for about 300 mountain and sub-polar glaciers world wide to statistically analyse changes in glacier regime over time. All averages have shown increasing tendency for negative mass balance starting in the mid-1970s, with an accelerating annual rate at the end of the 1980s (Figure 1.2). There has been an increase in global average equilibrium line altitude (ELA) of about 200 m (Figure 1.3) as well as a steady decrease in average accumulation area ratio (AAR) from around 60% to 50% (Figure 1.4). The data show increases in both ablation and accumulation, indicating increased summer temperatures and greater winter precipitation respectively. The average AAR appeared to be less than that for the average steady state AAR, implying that glaciers need to decrease surface area by about 7% to adjust to present climate conditions (Dyurgerov, 2003). These analyses show the need for ongoing effort into glacier monitoring, particularly volume change as this is the key variable that

is relevant to sea level rise.

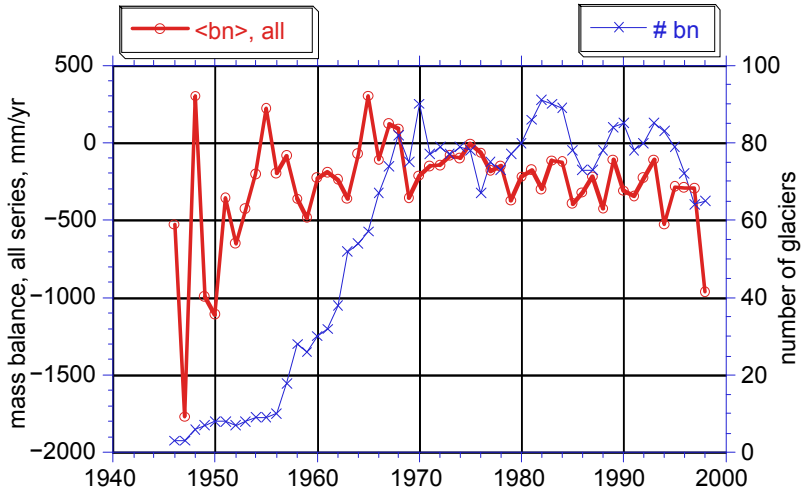

Figure 1.2: Mean of all WGMS glacier mass balance measurements, calculated annually since the record begins, along with the total number these glaciers for each year. Source: Dyurgerov (2002).

Other global glacier monitoring programmes include the Global Terrestrial Network for Glaciers (GTN-G) operating as part of the Global Climate Observing System (GCOS) and Global Terrestrial Observing System (GTOS). The GTOS project was designed to provide multidisciplinary quantitative information about the climate and Earth systems to facilitate change detection, modelling and prediction, understanding of ecosystems and environmental impacts, and to make the information available to the scientific community and policy makers (Haeberli et al., 2000; Haeberli, 2006). GTN-G implements monitoring strategies developed by WGMS and integrates the data with the World Glacier Inventory (WGI) for distribution by the National Snow and Ice Data Centre (NSIDC).

NSIDC is based in Boulder, USA and is the repository and distribution centre for global digital glacier data (National Snow and Ice Data Center, 2005). As well as facilitating the WGI, it facilitates and distributes processed and unprocessed imagery for the Global Land Ice Measurements from Space (GLIMS) project. GLIMS is a major contributor to both the GTN-G and the WGI. The ASTER sensor on board NASA's Terra satellite has provided imagery that has been acquired specifically for the GLIMS project.

New Zealand has not been a regular or significant contributor to any of these monitoring programmes despite the early work on the Ivory Glacier as part of the International Hydrological Decade (Anderton and Chinn, 1978).

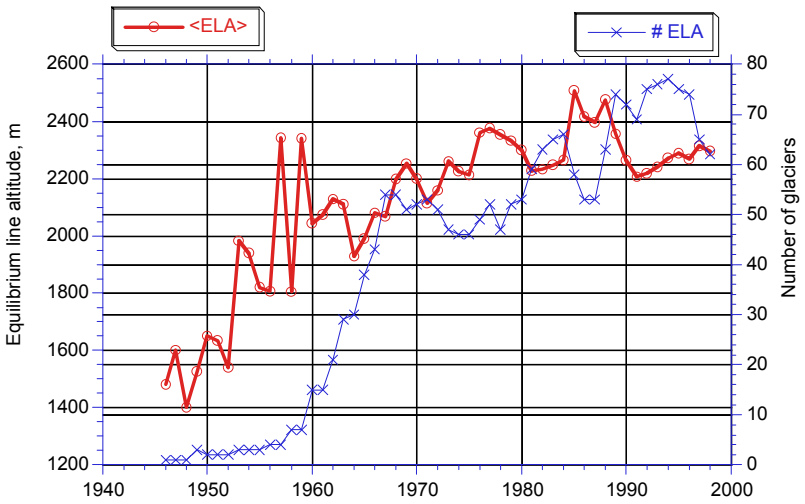

Figure 1.3: Equilibrium line altitude calculated as annual arithmetic means for all glaciers in the WGMS together with number of observations. Source: Dyurgerov (2002).

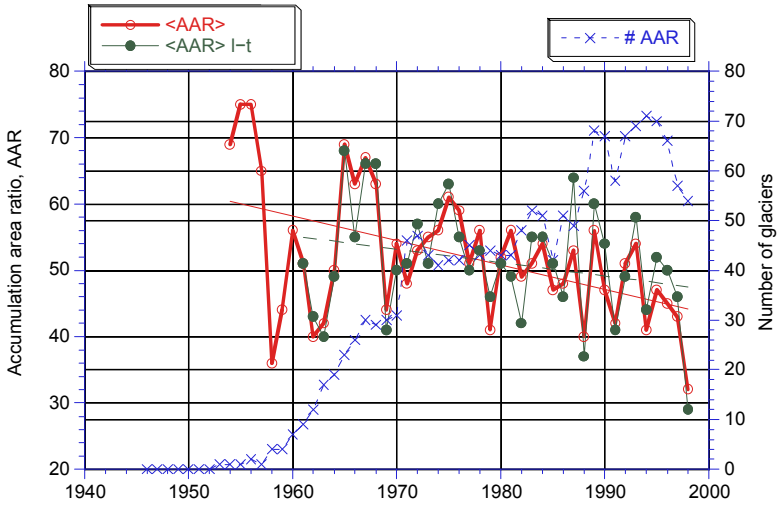

Figure 1.4: Accumulation-area ratio for all glaciers in the WGMS, and for long-term (l-t) records. Source: Dyurgerov (2002).

1.4 Glaciers and Glacier Change in New Zealand

1.4.1 Distribution of New Zealand Glaciers

New Zealand has a relatively large number of glaciers for the total area they occupy. This is due to the high number of peaks that reach just above the snowline. The 1989 New Zealand Glacier Inventory contained 3140 glaciers covering a total area of 1158 km^2 (Chinn, 1991). For the construction of the inventory, glaciers were defined as ice bodies of 1 ha or greater in area which have remained in existence during the most negative balance years over the past two decades.

The New Zealand land mass is elongated spanning 34° to 47° south latitude with mountains rising to 3754 m at Aoraki Mount Cook. The mountains run southwest to northeast forming a barrier to the prevailing west-southwest air flow (Salinger, 1980). This causes strong orographic uplift on the western side of the mountains and a steep precipitation gradient producing a föhn effect in the east (Griffiths and McSaveney, 1983). Precipitation is highly varied spatially from about 400 mm yr^{-1} in central Otago to 11,000 mm yr^{-1} in Fiordland (Tomlinson, 1992). The glaciers on the western side of the Main Divide are therefore far more active than those in the east. The maritime climate means that the temporal distribution of precipitation is fairly even throughout the year. Although temperatures are generally colder in the winter than summer, snow can fall year round (Tomlinson, 1992). Measuring mass balance is therefore more complicated than a continental system as the firn line of the previous year in the accumulation zones of the glaciers can be ambiguous. Measuring the end of summer snow line can also be difficult as the end of summer can be difficult to predict and may be unrepresentative. However, March to April is generally considered to be the end of summer (Chinn, 1995).

Most of the glaciers in New Zealand are situated along the Southern Alps of the South Island, with only 18 inventoried North Island glaciers, all on Mount Ruapehu.[1] Many of the glaciers are small cirque glaciers and glacierettes on separate peaks, with most of the glaciated area being within three main regions (Figure 1.5):

Aoraki Mount Cook region. At the centre of the Southern Alps, many of the peaks are well above the regional snowline. About 40% of New Zealand's glaciated area is in this region (Gjermundsen, 2007), including the majority of the valley glaciers.

Mount Aspiring region. Further south, this region contains relatively high altitude glaciers and ice plateaux. Much of the ice is stored around the edges of Mount Aspiring itself with other significant areas westward in the Olivine and Five Fingers Ranges and extending south into Fiordland.

Mt Evans, the Garden of Eden and Garden of Allah ice plateaux. This is an area of ice on the eastern side of the divide at the head of the Rangitata/Clyde Rivers in central Canterbury. The peaks in this region are barely above the regional snowline, but the topography is such that it accumulates a relatively large amount of snow. The small glacierettes in this region extend north to Arthur's Pass.

[1] There are now thought to be fewer than 18

The 1989 inventory was constructed largely from 1978 aerial photography and some significant changes have occurred since then. Gjermundsen (2007) remapped the ice cover in the Aoraki Mount Cook region based on a 2002 ASTER satellite image. This analysis covered 41% of the glaciated area in New Zealand and found an overall reduction of ice area from the 1989 inventory of 16.6%. However, it was suggested that actual volume loss was probably greater due to the downwasting of many of the valley glaciers on the eastern side of the divide.

1.4.2 Glacier Monitoring in New Zealand

The end of summer snowline (EOSS) survey (Chinn, 1995) is currently the only long-term glacier monitoring programme in New Zealand. Since 1977, oblique aerial photography has been used to annually measure the end of summer snowline altitude of 46 index glaciers, the locations of which are shown in Figure 1.6. EOSS has been shown to be an effective proxy for the equilibrium line altitude and can be used to estimate mass balance and the general health of the glaciers (Braithwaite, 1984; Kuhn, 1984; Paterson, 1994; Leonard and Fountain, 2003). The EOSS altitude has also been used for inferring glacier volume change. Chinn et al. (2007) have used a 30 year record of EOSS in New Zealand to construct a record of volume change. The EOSS is currently the only contribution from New Zealand to the WGMS. Chinn (2001) suggests that these data show the trend of recession since the end of the LIA has reversed, with glaciers overall showing positive balances since the survey began in 1977 (Figure 1.7). Although this is a significant data set, it is not appropriate for the world wide mountain glacier mass balance database that has been collated and analysed since 1997 by the Institute of Arctic and Alpine Research in Colorado who frequently point out the lack of data for New Zealand. GCOS have also called for more data from New Zealand (GCOS, 2004).

The longest complete mass balance record of a New Zealand glacier comes from the Ivory Glacier. Data were collected from 1969 to 1975 using a network of poles and showed consistently negative mass balance. The water and energy balances were also monitored. Soon after the programme began, a proglacial lake developed and there was a significant amount of loss due to calving into the lake (Anderton and Chinn, 1978). The Ivory Glacier is now virtually gone.

The Franz Josef Glacier on the western side of the divide has the most complete record of terminus position. The earliest known photograph of the terminus dates back to 1867 and regular observations have been made since. The terminus profile has been measured annually with a GPS receiver since 1996 and there has been some mass balance monitoring taking place in recent years.

Short term mass balance (for one or more years) has also been measured on the Whakapapanui (Thompson and Kells, 1973) and Brewster (George, 2005) Glaciers. Brewster Glacier is currently being monitored by Stumm (*pers comm*., 2007).

Satellite imagery has not been used as a method for measuring glacier volume change in New Zealand. Such methods may prove ideal for New Zealand glaciers and if successful would provide a valuable source of information for water resource management, climate modelling and sea level rise forecasts.

1.4.3 Tasman Glacier

Tasman Glacier is located Aoraki Mount Cook National Park and is the largest single glacier in New Zealand. It flows approximately south-east roughly parallel and immediately east of the Main Divide. There are many tributary glaciers that flow directly into the Glacier, the most significant being Ball, Hochstetter, Haast, Rudolf and Darwin Glaciers. The bulk of the ice in the lower half of the glacier comes from the Hochstetter, whose accumulation zone is on the eastern slopes of Aoraki Mount Cook (Kääb et al., 2002). Figure 1.8 shows the Tasman Glacier and its surroundings.

There are some sporadic records of glacier change from which volume change can be deduced, most notably the Tasman Glacier. The first recorded observations of glaciers in New Zealand are a set of sketches by the government surveyor Julius von Haast from his trip to the Mount Cook region in 1862 and included the terminus location of the Tasman Glacier (Grove, 2004; Burrows, 2005). However, Brodrick (1891a) later produced a high quality topographic map series in the 1880s and 1890s. In the process he measured surface elevation profiles across the main eastern valley glaciers including the Tasman, Murchison and Mueller Glaciers, and tracked boulders to determine their flow velocities (Brodrick, 1891b, 1894, 1906). Brodrick's surveys provide the most precise historical record of ice elevation change in New Zealand and his maps were only surpassed in quality after the introduction of photogrammetry in the 1950s (Gellatly, 1985). Skinner (1964) repeated two of Brodrick's surface elevation profiles of the Tasman Glacier in 1962 and found an average total surface lowering of 82.1 m. Intermittent mass balance measurements occurred from 1957 until 1975 (Goldthwait and McKeller, 1962; Anderton, 1975) and surface lowering was again examined by Kirkbride (1989) from 1985 to 1987, Ruddell (1995) in 1991 and Watson (1995) in 1994. Watson concluded that average surface elevation across Brodrick's Ball Hut profile was 157 m lower in 1995 than in 1890. The Tasman Glacier also has the longest EOSS record beginning in 1966.

Maps of the Tasman Glacier and the Aoraki Mount Cook region are the oldest of any glaciers in New Zealand. However, it was not until Brodrick that quantitative topographic surveys were made. Several transects of the Tasman Glacier were surveyed in 1890 by Brodrick (1891b) and were included in his topographic map published the following year (Figure 1.9). He measured surface elevation along the transects for the purpose of establishing long term volume change. Brodrick's foresight provides the first instrumental record for calculating glacier volume change of glaciers in New Zealand.

The two transects D and C have been resurveyed several times since Brodrick. Watson (1995) compiled the data of repeated surveys up until 1990 (Hochstein et al., 1995) and then added his own in 1993 and 1994. Two more were completed for this study in 2007 using a differentially corrected GPS, with an average accuracy of approximately 20 cm. A correction factor was applied to the elevation data to adjust for the slightly different paths of the transects between dates. Watson (1995) determined the distance north to south from each point to the average northing of his 1994 transect. He then assumed a surface slope of 0.0349 to estimate the elevation at this datum line. This correction factor was applied to the transects for all years. The adjusted elevation profiles can be seen in Figures 1.10 and 1.11.

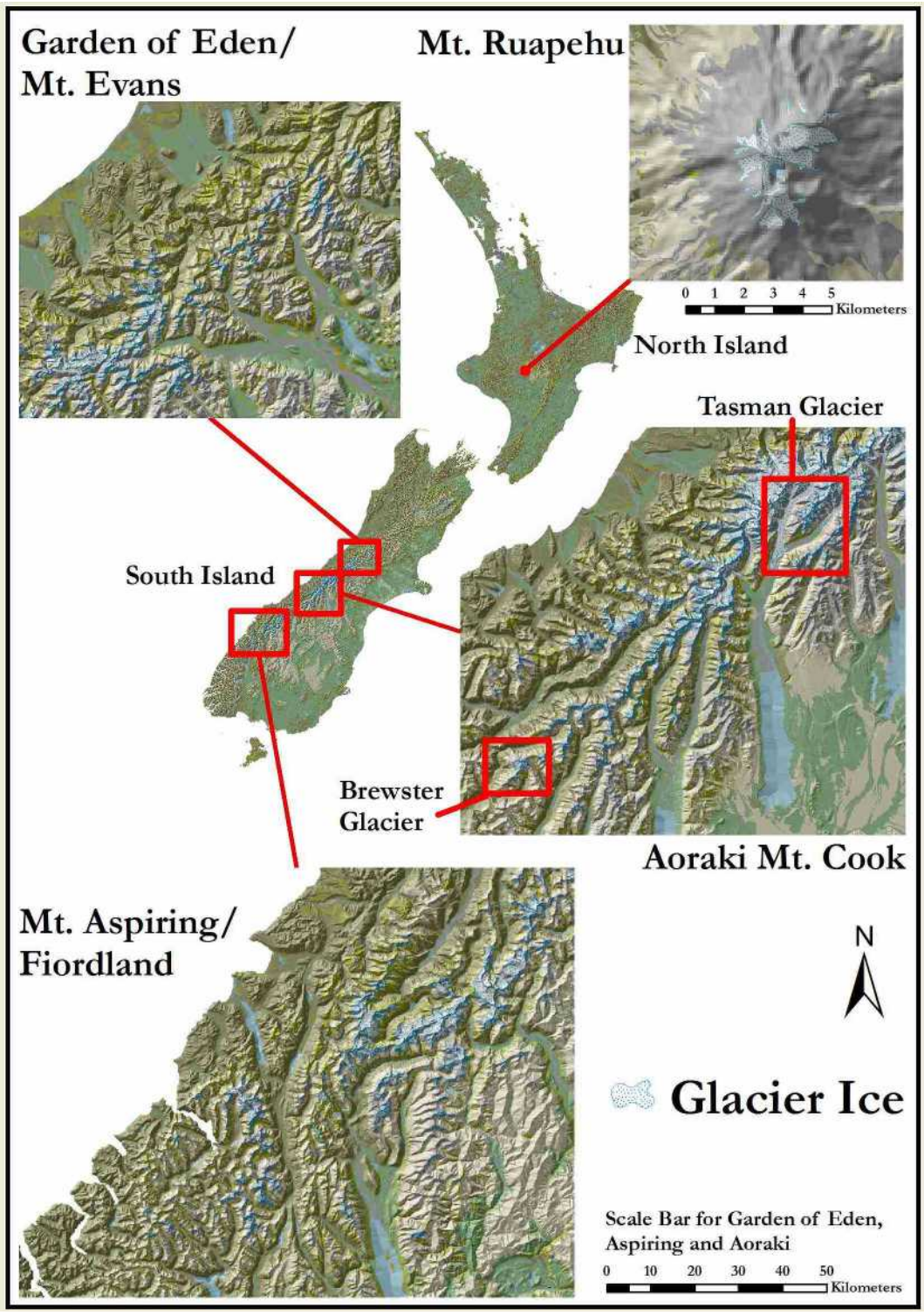

Figure 1.5: The distribution glaciers in New Zealand. Note that the scale for the Ruapehu region is larger than the other three regions.

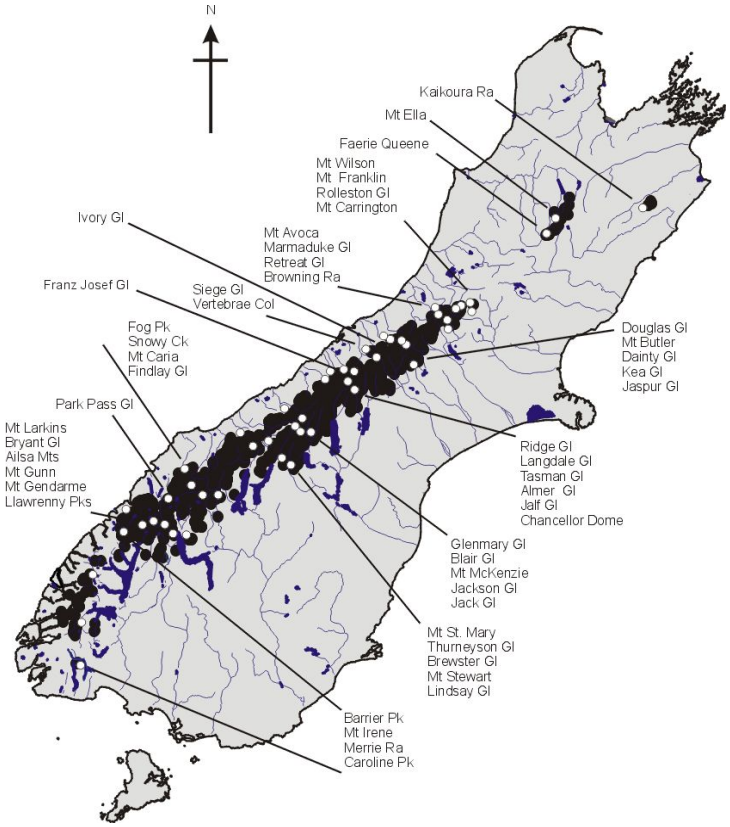

Figure 1.6: Distribution of the 46 index glaciers used in the New Zealand Glacier Snowline Survey. From Chinn (2001).

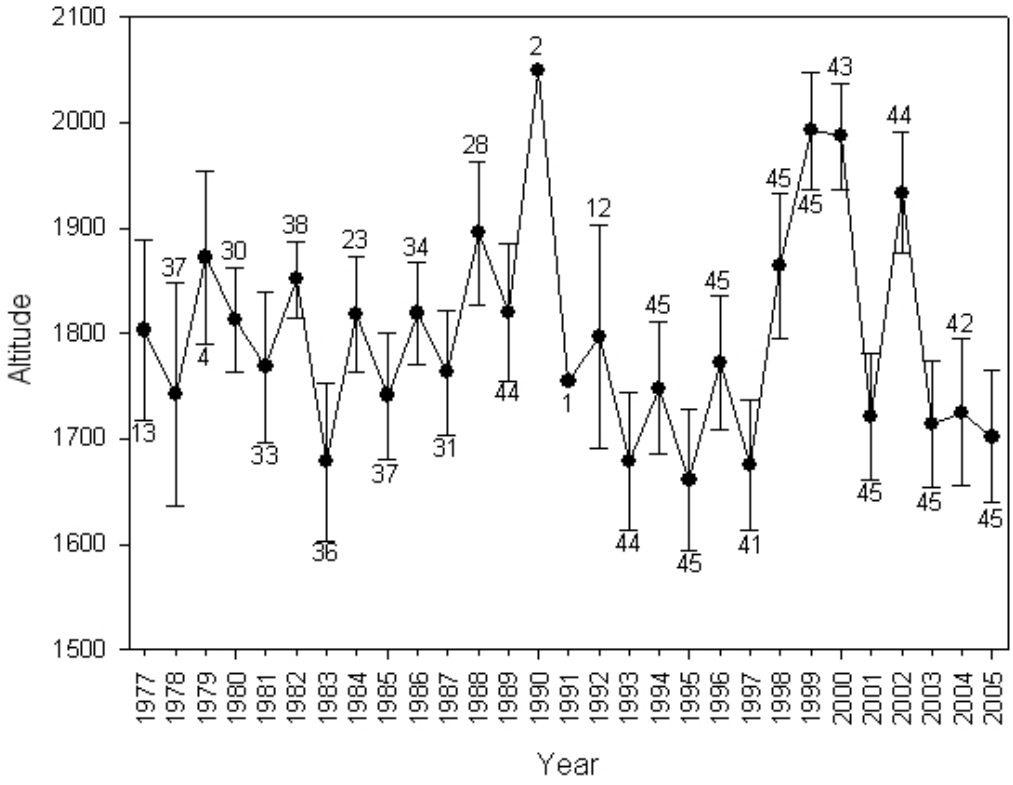

Figure 1.7: Changes in average EOSS 1977–2005, with 95% confidence limits and number of EOSS index glacier measurements. Estimates for the 1989/90 year are only from two index glaciers, and one index glacier observation from 1990/91. Source: Chinn et al. (2007).

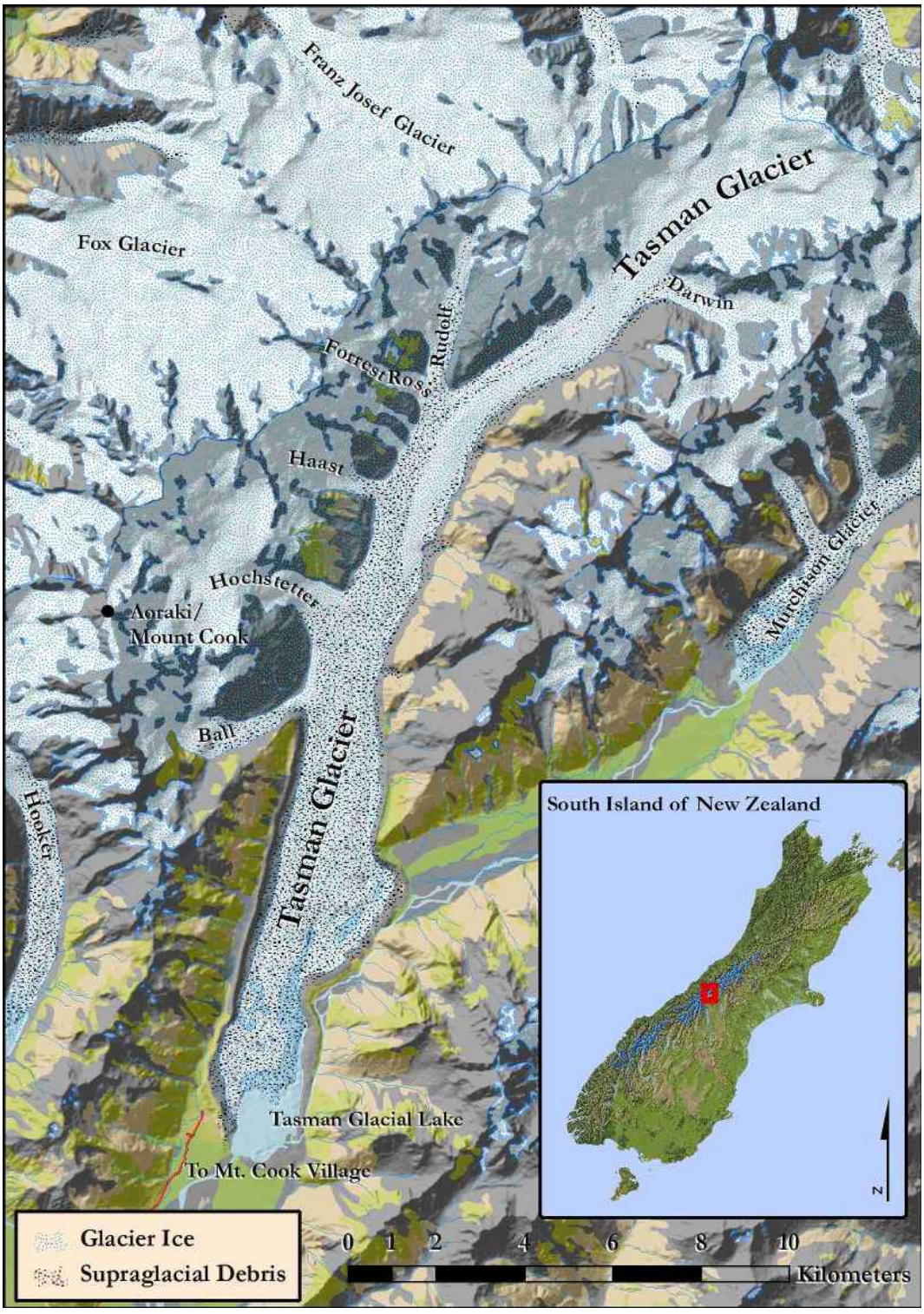

Figure 1.8: The Tasman Glacier and its tributaries.

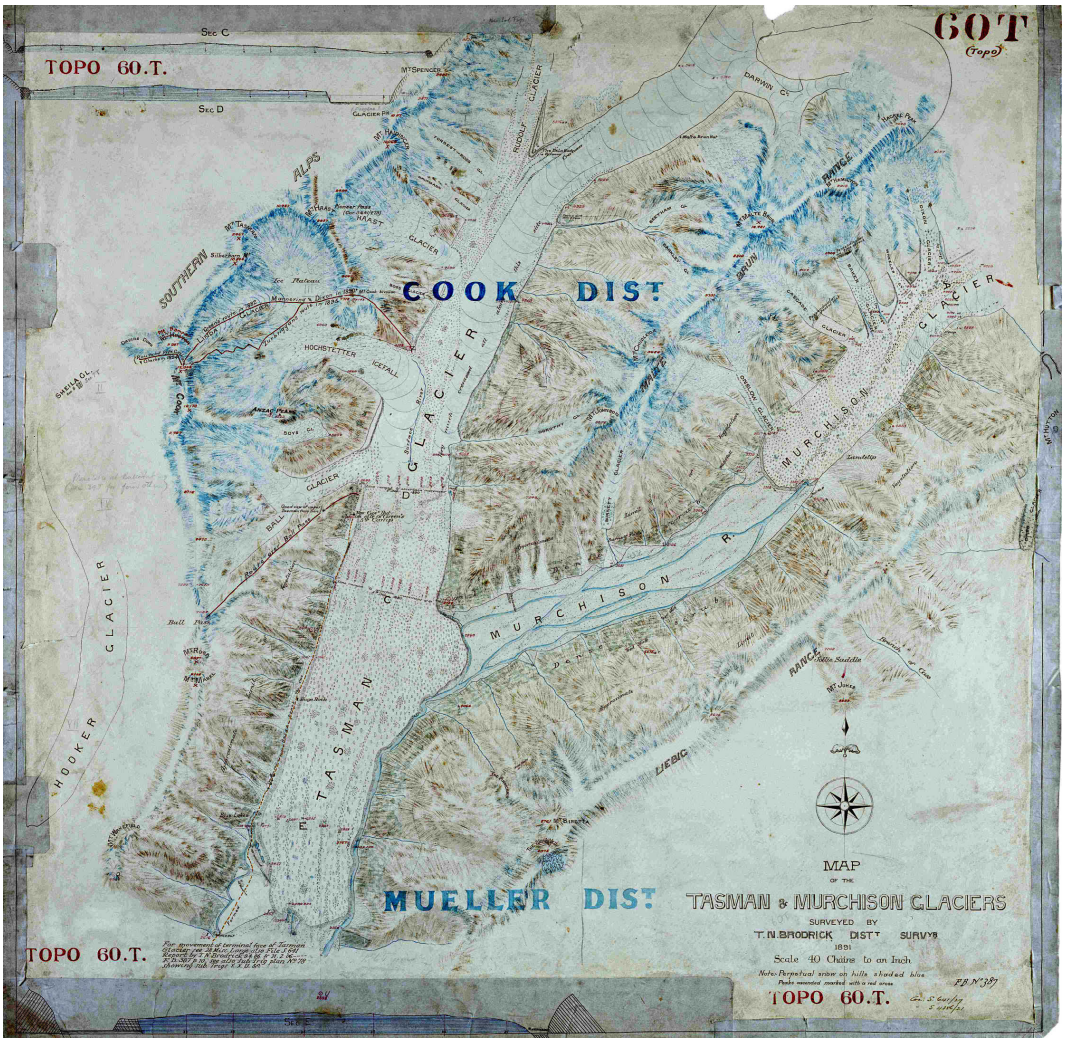

Figure 1.9: Noel Brodrick's topographic map of the Tasman Glacier, 1891. The transects can be seen as two straight lines marked across the glacier at approximately the middle of the map, with the Ball Hut transect being the upper line – transect D, and Malte Brun Corner being the lower – transect C. (Brodrick, 1891a)

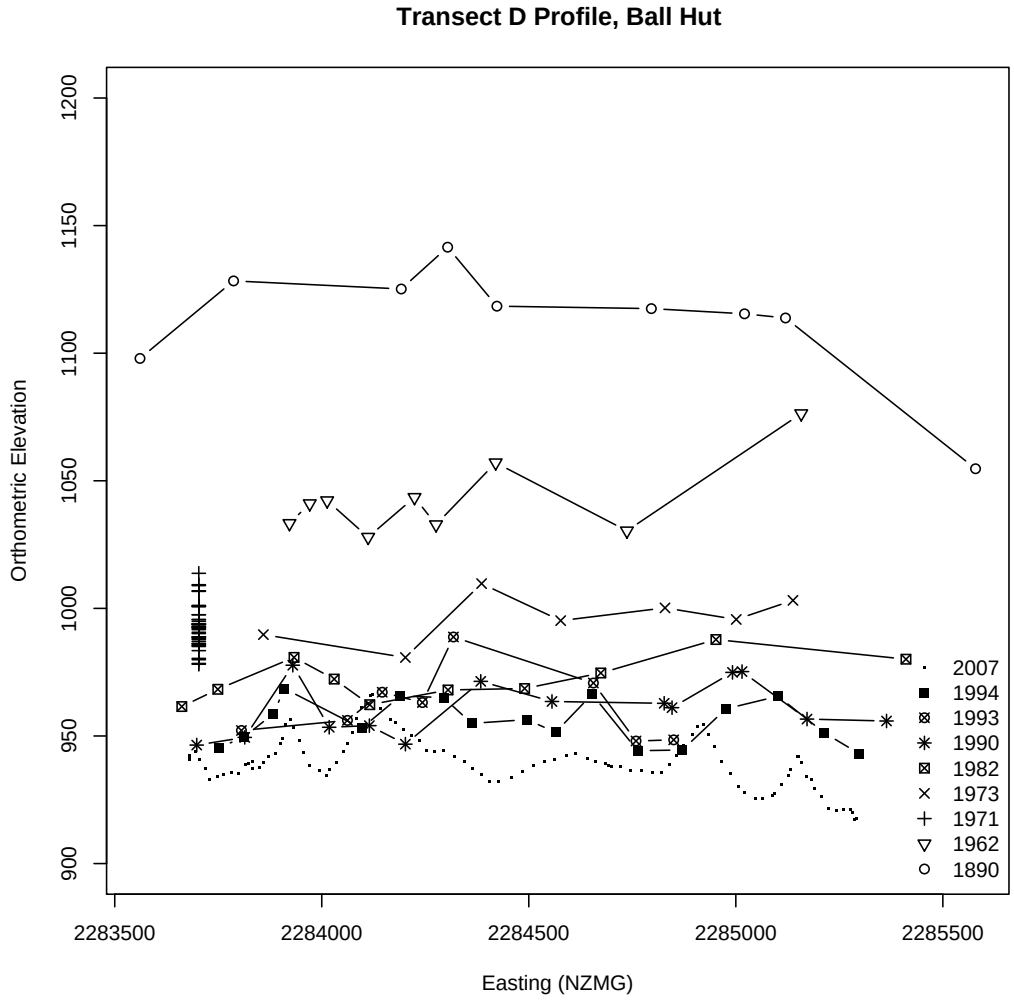

Figure 1.10: Profile view of the Ball Hut transects showing the surface elevation along each transect. Coordinates of the 1971 measurements were not recorded and therefore show the range of elevation values at the starting location.

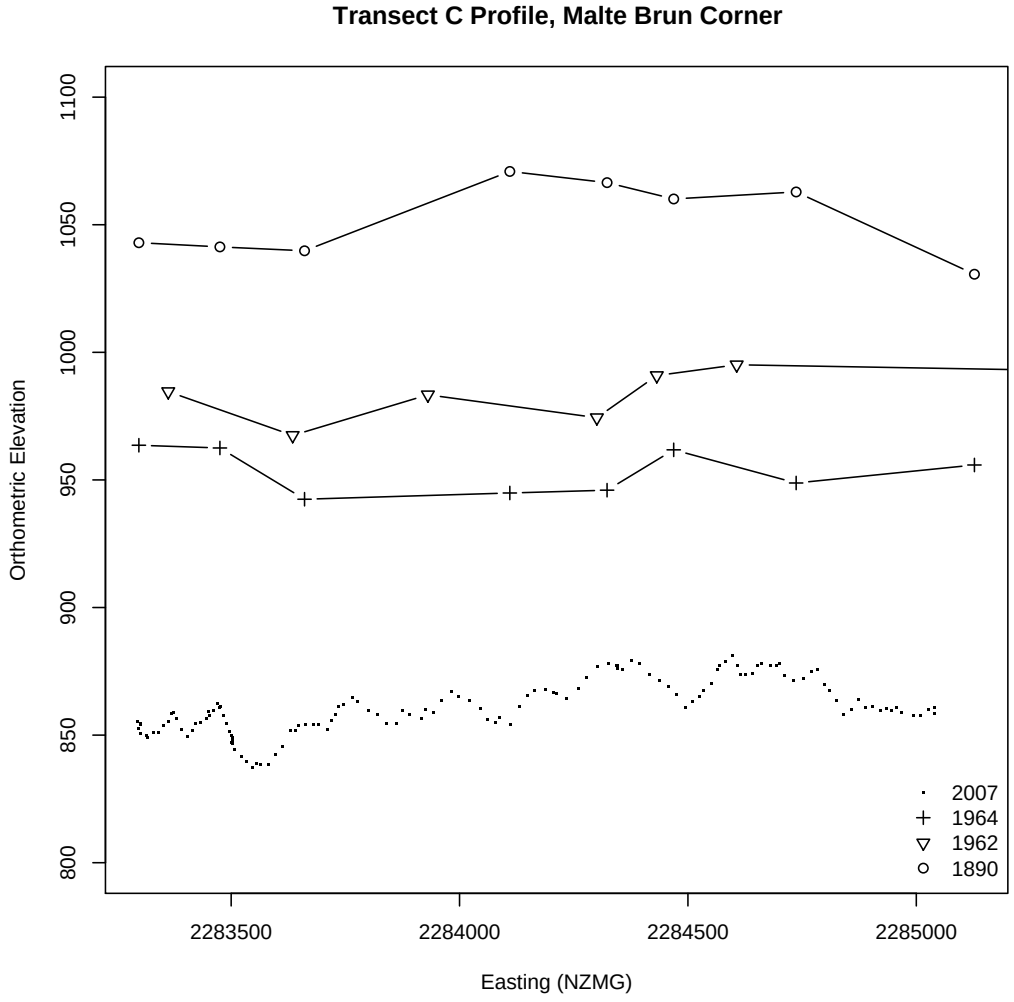

Figure 1.11: Profile view of the Malte Brun transects showing the surface elevation along each transect.

.

1.5 Aims

The overall aims of this research are to:

- Explore the possibility of using remotely sensed data to extract topographic data from the Tasman Glacier.
- Test the reliability of the extracted topographic data for determining volume change of the Tasman Glacier.

Chapter 2

Extracting Topographic Data

2.1 Introduction

Elevation data for Tasman Glacier region were obtained for five different years from several different data sets:

1965 & 1986 – Photogrammetry: aerial photography for these two years provided the means to extract elevation data using digital photogrammetric techniques.

1986 – TOPODATA DEM: topographic maps were originally produced of the region using analytical plotters and were later digitised to make the TOPODATA topographic database. Contour lines and spot heights were interpolated to a DEM by Barringer et al. (2002) . This DEM is considered the most accurate and complete data set available and is used here as a datum state.

2000 – SRTM: an extract from the global SRTM DEM data set, which was acquired using radar from the Space Shuttle Endeavor, was obtained from NASA. This DEM provides near global coverage and is therefore a globally consistent data set.

2002 & 2006 – ASTER imagery: stereo pairs from the ASTER sensor on board NASA's Terra satellite were used to extract data points using the same techniques as for 1965 & 1986.

Table 2.1 gives an overview of data sets used. This chapter discusses in detail these data sets and the methods used to derive topographic data from them.

Table 2.1: Overview of data sets used for this study.

Data Set	Year	Data Type
SN1580	1965	Aerial Photography
SN8595	1986	Aerial Photography
TOPODATA	1986	Digital Elevation Model
SRTM	2000	Synthetic Aperture Radar
AST2002	2002	ASTER Optical Satellite Imagery
AST2006	2006	ASTER Optical Satellite Imagery

2.2 Aerial Photography and ASTER Imagery

The data extraction procedures were similar for the aerial photography and ASTER satellite imagery and are therefore described here together.

2.2.1 The Aerial Photography

Two blocks of photogrammetric quality aerial photography were used to derive elevation data. These give coverage of the Glacier for the years 1965 and 1986. Details of these photographs are given in Table 2.2.

Table 2.2: Aerial photographs used to extract topographic data.

Survey Number	Survey Date	Nominal Scale	Print Numbers
SN1580	19/03/1965	1:67,000	3723/33-39, 3724/29-37
SN8595	01/02/1986	1:50,000	A10-A13, B10-B13, C16-C18

Due to the timing of obtaining the photographic prints and the availability of suitable scanners, the SN 1580 photographs were scanned using a Microtek 9800XL scanner and the SN 8595 photographs were scanned using an Epson Expression 10,000XL, all at an optical resolution of 1200 dpi. Figures 2.1 and 2.2 show orthorectified mosaics of the scanned aerial photographs for 1965 and 1986 respectively.

2.2.2 The ASTER Imagery

Two satellite images from the Advanced Spaceborne Thermal Emission Reflection Radiometer (ASTER) sensor for the years 2002 (Figure 2.3) and 2006 (Figure 2.4) were obtained, being the most suitable

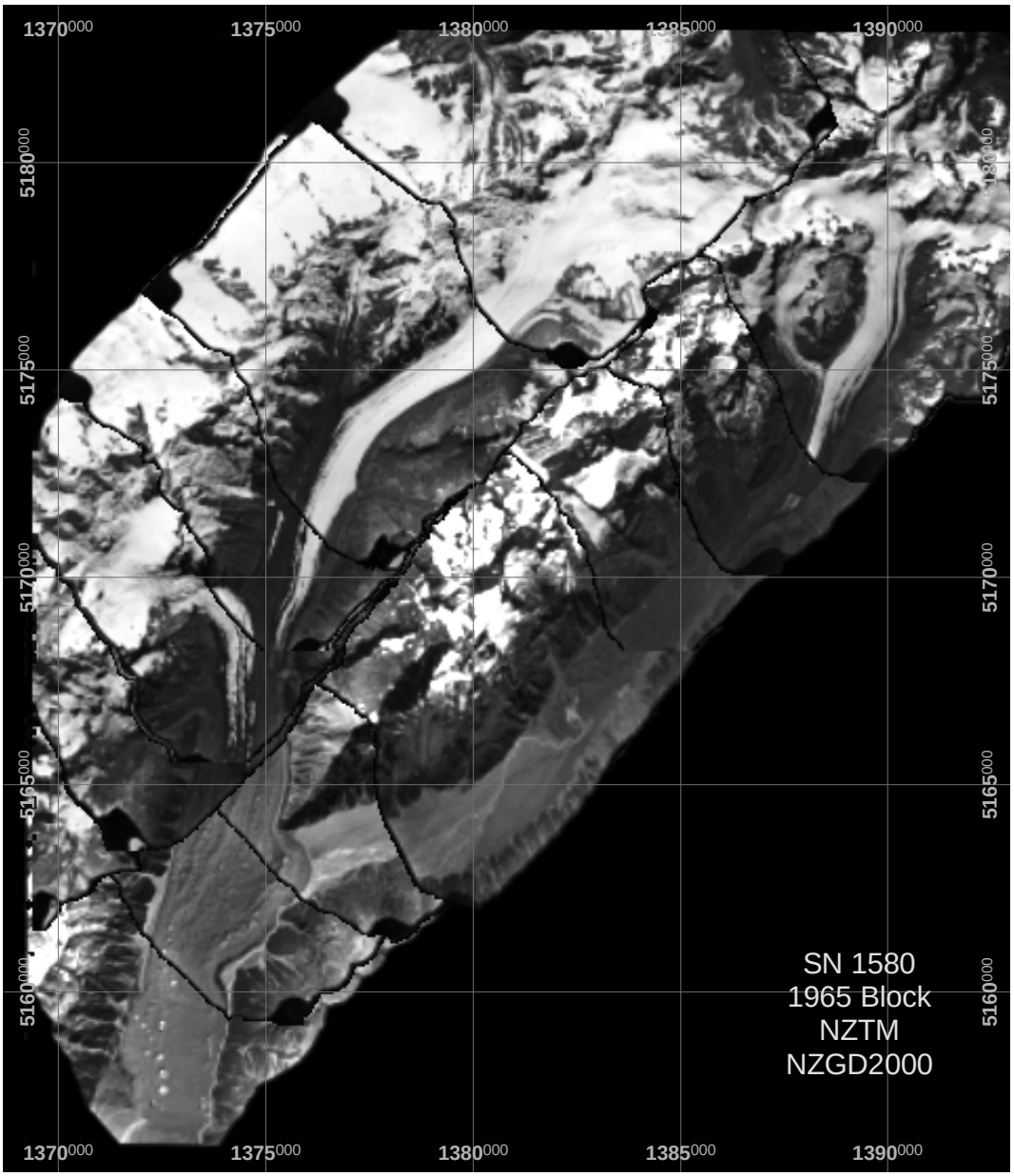

Figure 2.1: Orthorectified mosaic of SN 1580 1965 aerial photographs.

summer images available of the glacier with low cloud cover and high gain. ASTER provides optical stereo imagery which has shown to be highly effective for glacier monitoring (Kääb et al., 2002; Kääb, 2002; Cheng et al., 2003; Kamp et al., 2003; Vignon et al., 2003; Khalsa et al., 2004; Bolch et al., 2005; Rivera et al., 2005; Stearns and Hamilton, 2005).

The ASTER instrument has three separate sensors: the visible near-infrared (VNIR), shortwave-infrared (SWIR) and thermal-infrared (TIR) radiometers with a swath width of 60 km (Table 2.3) .

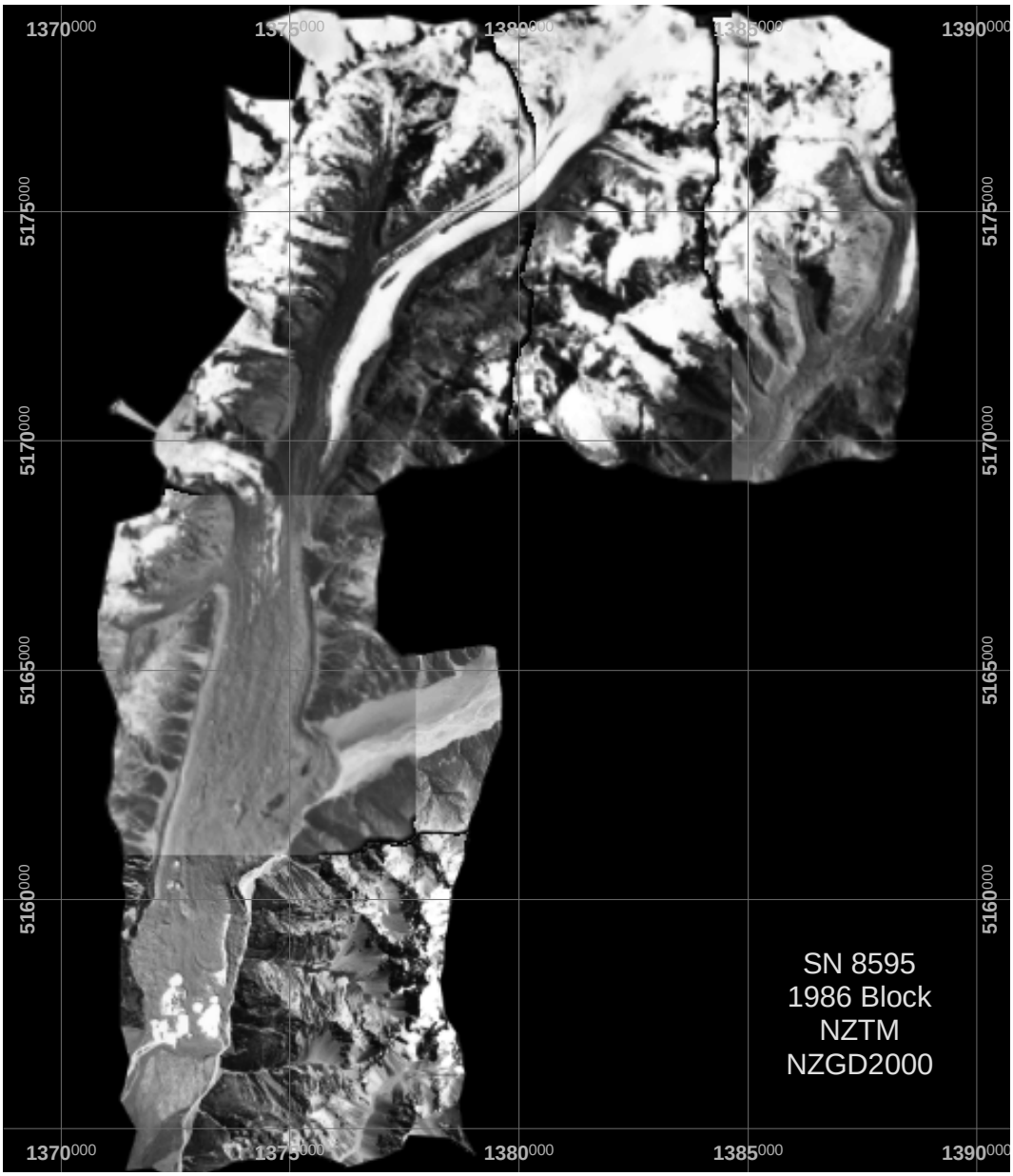

Figure 2.2: Orthorectified mosaic of SN 8595 1986 aerial photographs.

The VNIR band three provides along-track stereo coverage with the combination of nadir (band 3N) and backward looking (band 3B) acquisition with a base to height ratio of 0.6, enabling DEMs to be produced. Figure 2.5 shows the geometry of image acquisition for stereo pairs from the ASTER sensor. ASTER is carried on board the Terra satellite as part of NASA's Earth Observing System (EOS) along with four other sensors.

Terra has a sun synchronous orbit at 705 km above the Earth's surface and crosses the equator on

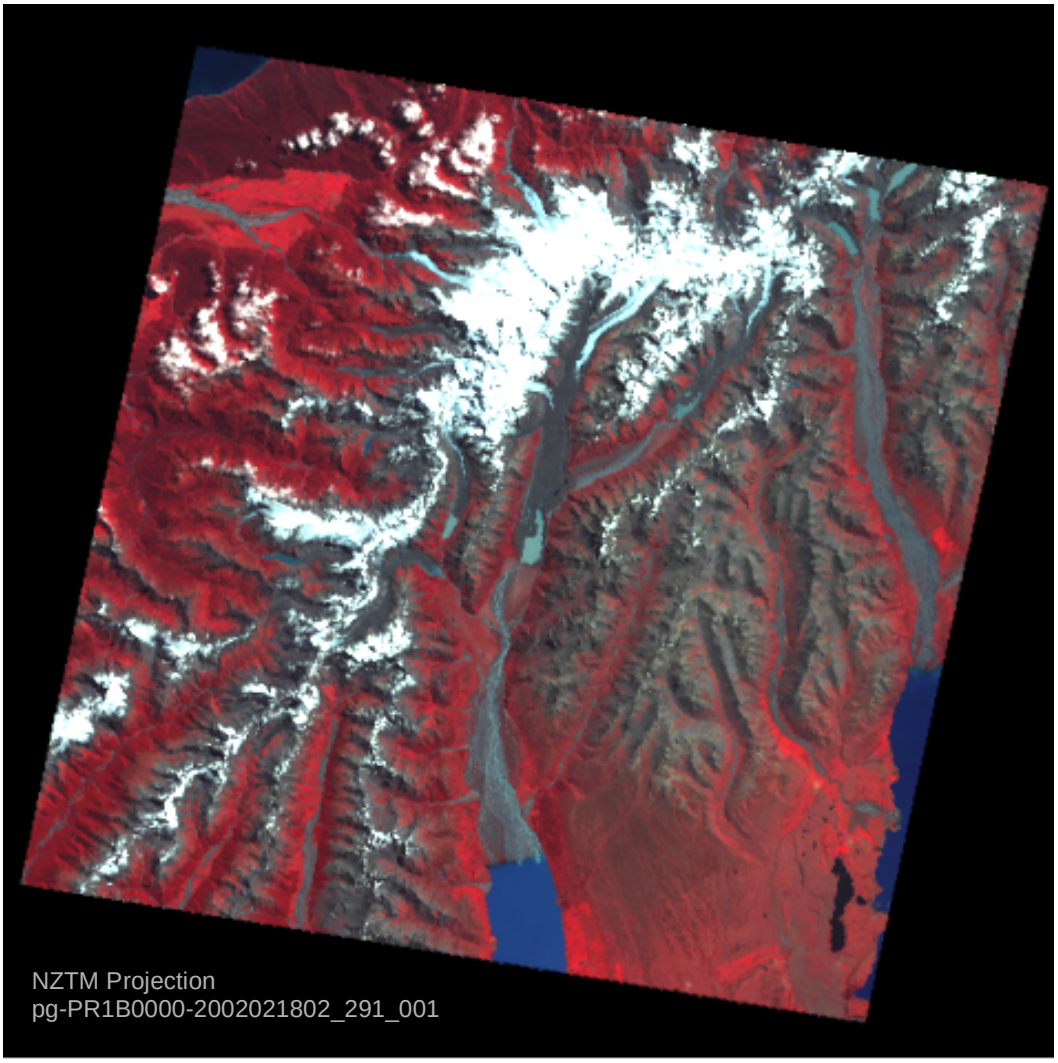

Figure 2.3: ASTER false colour infrared preview image from 2002.

descending passes at 10:30 AM with a repeat cycle of 16 days NASA (2006). The timing is designed to coincide with the least amount of cloud cover obscuring visibility of the Earth's surface, but has the disadvantage of the sun being at a low azimuth projecting significant shadows in steep mountain topography, which is typically where glaciers are located.

Distortion parameters for the ASTER imagery were provided with the meta data of the images. The images were obtained at Level 1A, which required destriping and the digital numbers being converted to radiance.

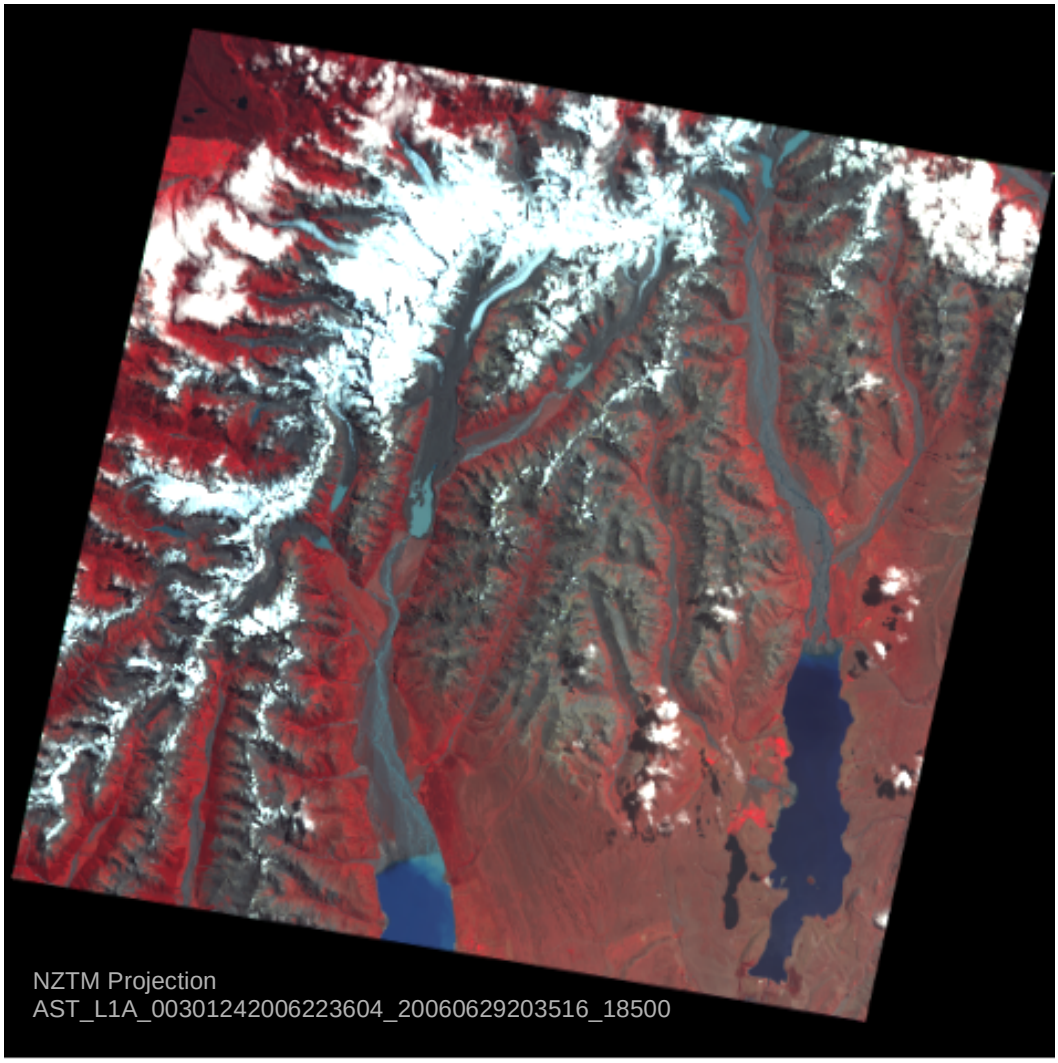

Figure 2.4: ASTER false colour infrared preview image from 2006.

2.2.3 Extracting Elevation Data

Data were extracted from stereo pairs of the vertical aerial photography and ASTER imagery using digital photogrammetry techniques. Leica Photogrammetry Suite (LPS) provided the tools to extract elevation data, with ground control points (GCPs) providing the basis for the triangulation models.

Ground Control Points

GCPs were collected around the glacier to establish accurate geolocation of the aerial photographs for the aerial triangulation model. As many GCPs as was practically possible given the hazardous terrain of the region were collected using GPS. GCPs were collected using a differentially corrected

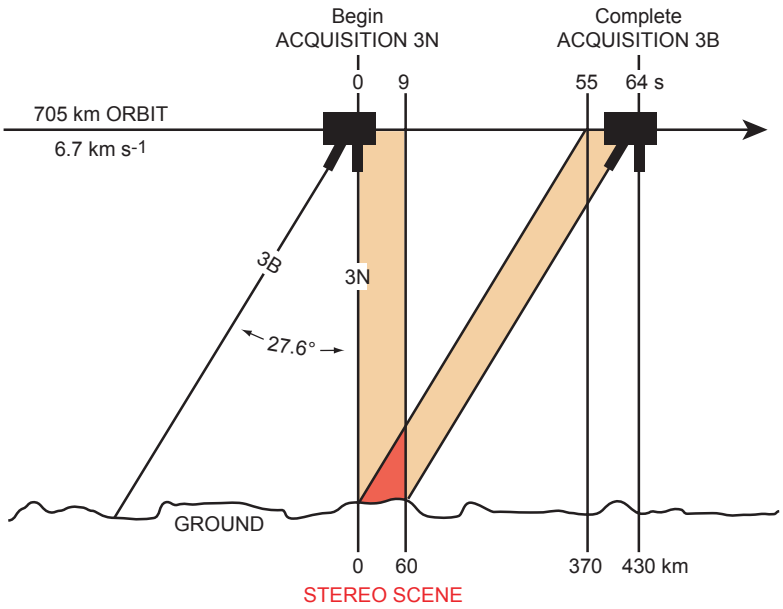

Figure 2.5: Geometry and timing of ASTER's nadir 3N band and backward looking 3B band, which together form a stereo pair. From Kääb et al. (2002).

Trimble R8 GPS at sub-centimetre accuracy, in terms of the NZTM Projection, NZGD2000.

Additional GCPs were digitised from the 1:50,000 topographic map database in order to produce an adequate model. Their precise co-ordinates were obtained from within ArcGIS using the TOPODATA DEM (Section 2.3) for z co-ordinates in NZMG and converted to NZTM with a precision of approximately 20 cm. Most of the same GCPs were used in all four data sets to maximise their relative accuracies. The location of the GCPs in relation to the aerial photographs are shown in Figures 2.6 and 2.7. Figures 2.8 and 2.9 show the same for the ASTER imagery.

Block Definition

Leica Photogrammetry Suite was used for processing the aerial photos and ASTER images, as it provides the tools to process digital photogrammetric data in place of analogue systems such as analytical plotters. Although LPS only operates on a single stereo model at a time, it enables the definition of entire blocks, simultaneously integrating many stereo models seamlessly (a stereo model is a pair of overlapping stereo images and a block is a set of contiguous stereo models).

Camera calibration reports were provided with the aerial photography, which contained information relating to distortions and imperfections of the lens installed on the camera that took the photographs (interior distortions). This information was used in defining the two blocks of aerial photographs to compensate for their distortions. The fiducial marks were located on the images to a RMSE of less than 3 μm in all cases. After the GCPs were defined the tie points were located. Tie points are defined in the same way as GCPs in that they link the same location on two overlapping images, but are treated as unknown co-coordinates. The aerial triangulation process

Table 2.3: Characteristics of the ASTER sensors. Modified from Yamaguchi et al. (1998).

Sensor	Band No.	Spectral Range (μm)	Absolute Accuracy (σ)	Spatial Resolution
VNIR	1	0.52-0.60	$\leq \pm 4\%$	15 m
	2	0.63-0.69		
	3N	0.78-0.86		
	3B	0.78-0.86		
SWIR	4	1.600-1.700	$\leq \pm 4\%$	30 m
	5	2.145-2.185		
	6	2.185-2.225		
	7	2.235-2.285		
	8	2.295-2.365		
	9	2.360-2.430		
TIR	10	8.125-8.475	$\pm$ 3K(200-240K)	90 m
	11	8.475-8.825	$\pm$ 2K(240-270K)	
	12	8.925-9.275	$\pm$ 1K(270-340K)	
	13	10.25-10.95	$\pm$ 2K(340-370K)	
	14	10.95-11.65		

was performed using Brown's Physical Model, which compensates for 14 distortion parameters of both the interior and exterior (exterior parameters relate to factors independent of the camera such as atmospheric and terrain distortions) The aerial triangulation process employs the Least Squares Adjustment method and performs automatic bundle adjustment to establish the relationship between the aerial photographs and the NZTM map projection, providing geographic coordinates for each tie point.

Automatic Terrain Extraction

Elevation data for all blocks (both the aerial photography and satellite imagery) were extracted using the Automatic Terrain Extraction (ATE) module in LPS. The ATE process searches for corresponding pixels in each image of a stereo model at a given spacing (x m), in this case 5 m for the aerial photography and 45 m for the ASTER imagery. The GCPs and tie points were used as seed points for this process, meaning that searching began from these points working outwards along the epipolar line. Extra points selected from TOPODATA (Section 2.3) representing rock surfaces were included as seed points to improve the accuracy of the point matching process. Each time the algorithm moves x m along from a seed point in the left image, it searches along the epipolar line (which has been determined from the triangulation process) for the corresponding pixel in the right image. A moving window is used to to assess surrounding pixels and after finding a possible match, decides whether

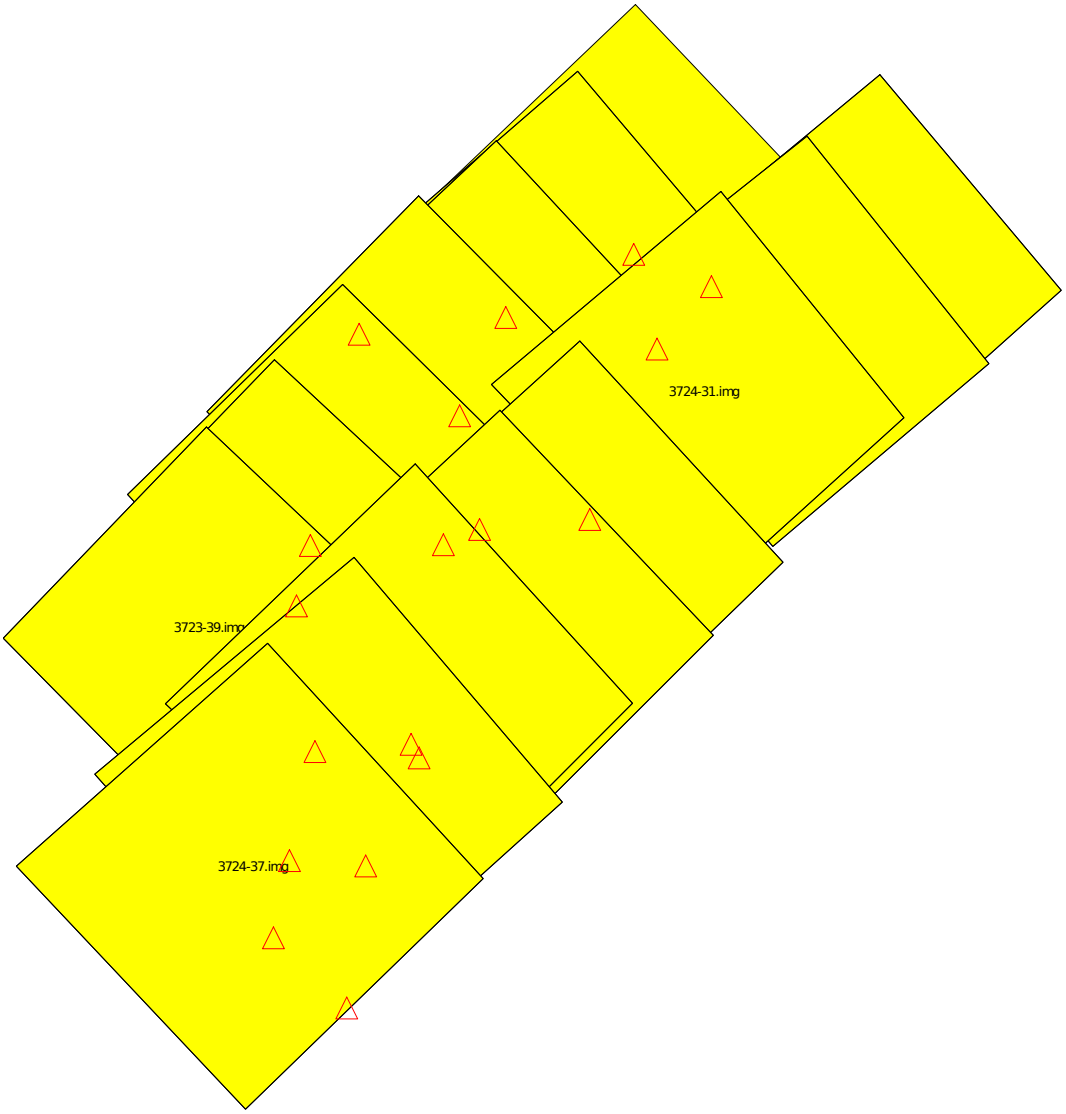

Figure 2.6: SN 1580 (1965) block diagram. Yellow squares represent orientation of the aerial photographs with GCPs indicated by red triangles.

or not to accept a point based on the r^2 of the pixels within the window of each image. The parallax between the two corresponding pixels is then measured to give that point a geographical co-ordinate (Leica, 2006). This process is based on the work by Keating et al. (1975). A problem with this approach is that after if a wrongly matched point is accepted, the error propagates outwards along the search line. The further the moving window gets from a seed point without making a correct match, the greater the resulting error is likely to be when a match is finally made. To try to reduce error propagation, a threshold for r^2 was set at 0.80 to minimise the number of low quality points. However, this also has the effect of increasing the relative frequency of isolated points.

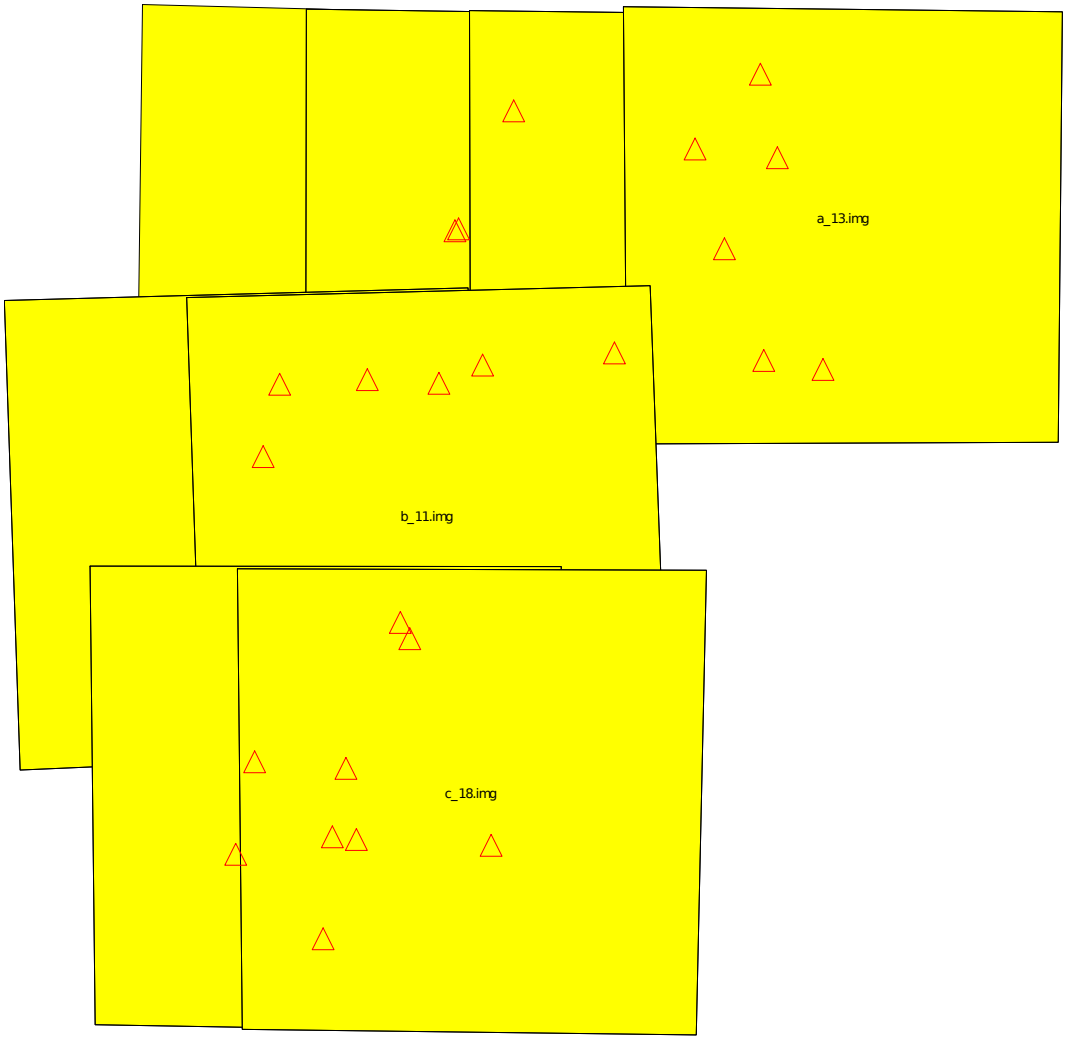

Figure 2.7: SN 8595 (1986) block diagram. Yellow squares represent orientation of the aerial photographs with GCPs indicated by red triangles.

The *mass points* from the correlation process form the basis for the production of a DEM. The resulting point spacing is related to the number of seed points and the number of points accepted in the process. A regular grid raster DEM is constructed from the mass points by interpolating between them using delauny triangulation (linear interpolation). This interpolation method was not satisfactory, as it produced a topography of triangles with isolated points producing large spikes in the surface. It was decided that working with a cloud of discrete mass points would produce better results by enabling errors to be removed by comparing it to the TOPODATA DEM.

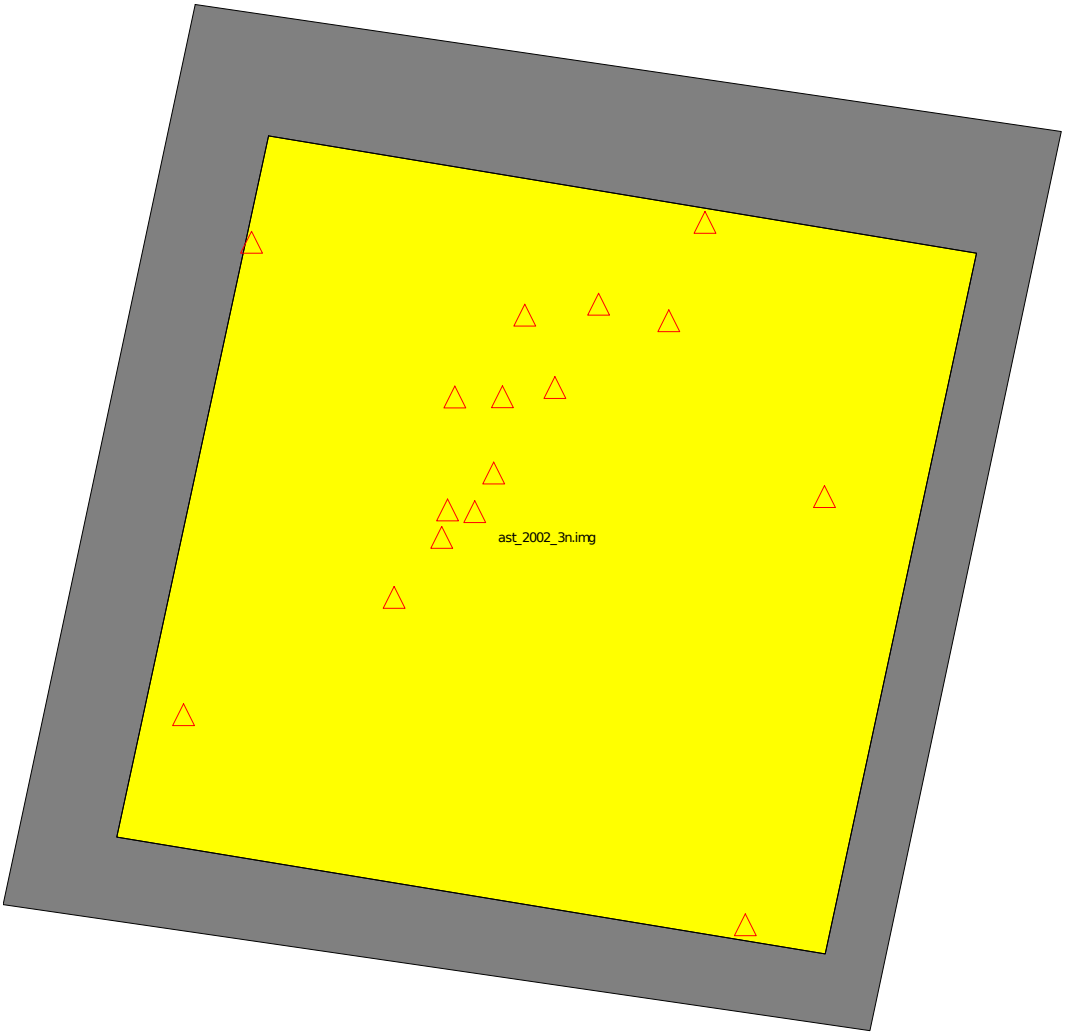

Figure 2.8: ASTER 2002 block diagram. The yellow square shows the region of overlap between the two stereo pairs with GCPs indicated by red triangles.

Table 2.4: Accuracy of the aerial triangulation and ATE process.

Block	GCPs	Tie Points	Triangulation RMSE (metres)	DTM RMSE (metres)
SN 1580	18	3324	3.14	±16.71
SN 8595	24	13596	1.50	±16.58
AST 2002	16	2639	0.03	±42.87
AST 2006	15	1710	0.06	±68.92

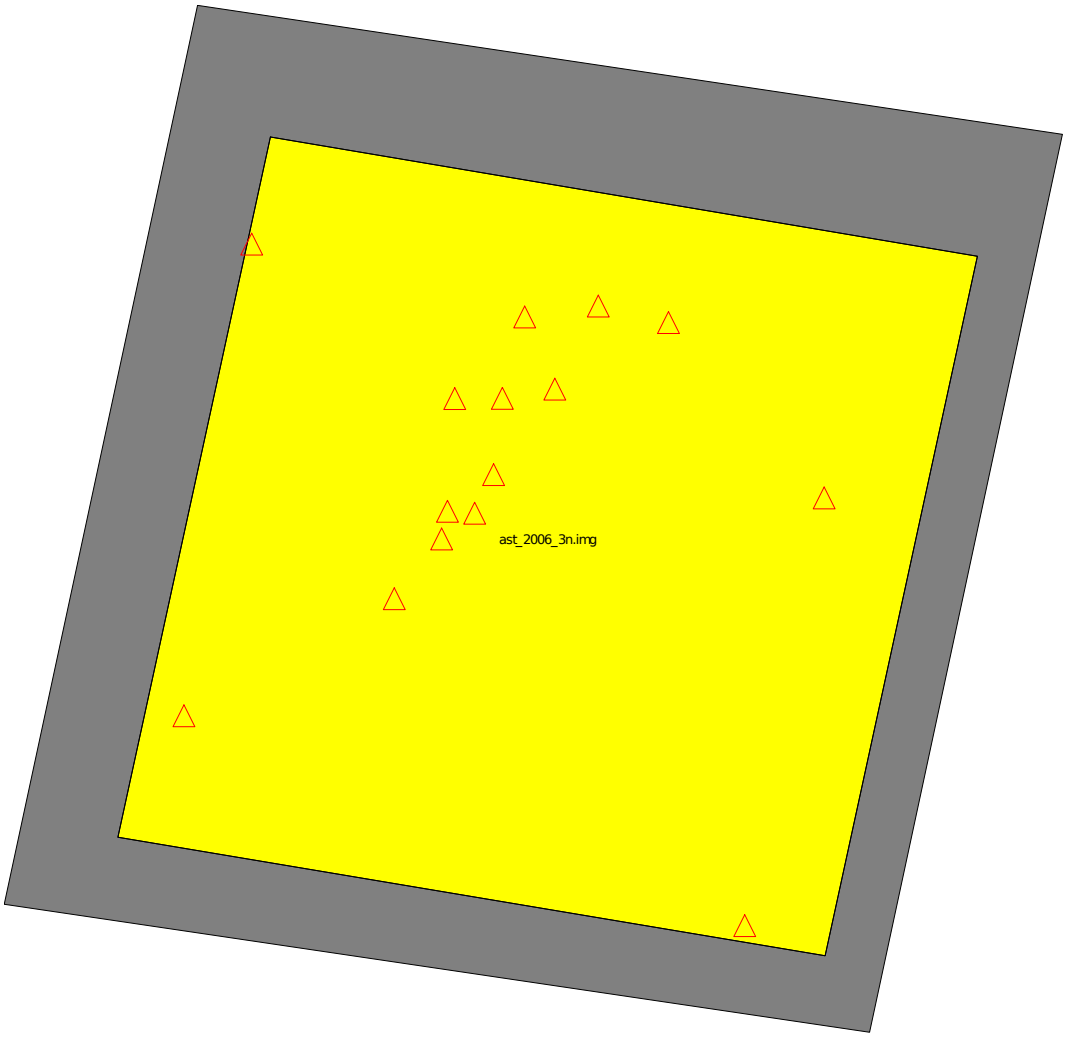

Figure 2.9: ASTER 2006 block diagram. The yellow square shows the region of overlap between the two stereo pairs with GCPs indicated by red triangles.

2.3 TOPODATA

Barringer et al. (2002) constructed a DEM from the TOPODATA topographic database of New Zealand and was used in this study as a datum state for comparing all other data sets. The New Zealand Topographic Map 260 Series, published by Land Information New Zealand at a scale of 1:50,000, was produced using analytical plotters with the same aerial photography as was used in this study – 1986 SN 8595, and therefore provides elevation data for 1986. However, the Tasman Lake extent is modified to reflect the 1993 lake extent. The original paper maps were subsequently digitised to make the TOPODATA database. Barringer et al. (2002) used the spot heights and 20 m spaced contour lines from TOPODATA to create a DEM at 25 m resolution and 32 bit floating point precision. The interpolation algorithm was custom made for the purpose of most accurately representing the surface defined by the contour lines and spot heights. This resulting DEM was compared to 2700 GPS points and a LIDAR DEM that covered a range of landform types. The RMSE was shown to be 6.15 m using the GPS points and 5.13 m using LIDAR (Barringer et al., 2002). Figure 2.10 shows a hillshade of a subset of the DEM covering Tasman Glacier, which is currently the best available for the region.

The TOPODATA DEM was reprojected from NZMG to NZTM and heights adjusted from orthometric (Lyttelton Datum) to NZGD2000 ellipsoidal with an estimated accuracy of approximately $\pm$20 cm.

Figure 2.10: Hillshade of the DEM made by Barringer et al. (2002) from TOPODATA contour lines and spot.

2.4 Shuttle Radar Topography Mission Data

Elevation data from the Shuttle Radar Topography Mission (SRTM) provided good coverage of the Tasman Glacier for February 2000. The SRTM data were acquired using synthetic aperture radar from the Space Shuttle Endeavour and has provided the first globally uniform DEM of the Earth

between 60° north and 56° south. Both C band (λ5.6 cm) and X band (λ3.1 cm) measurements were carried out to produce DEMs with 3×3 arc second and 1×1 arc second spacing respectively. SRTM data has been widely used for measuring glacier surface elevations and volume change (Vignon et al., 2003; Berthier et al., 2004, 2006; Aizen et al., 2007; Larsen et al., 2007; Schiefer et al., 2007; Muskett et al., 2008).

C band data set `S44E170.hgt` covering the Tasman Glacier was projected to NZTM using the NZGD 2000 datum, giving a point spacing of approximately 61×92 m. There were some large holes in the data, mainly in the extreme high altitude glaciated areas which can be seen in Figure 2.11. However, coverage of the Tasman Glacier surface was complete.

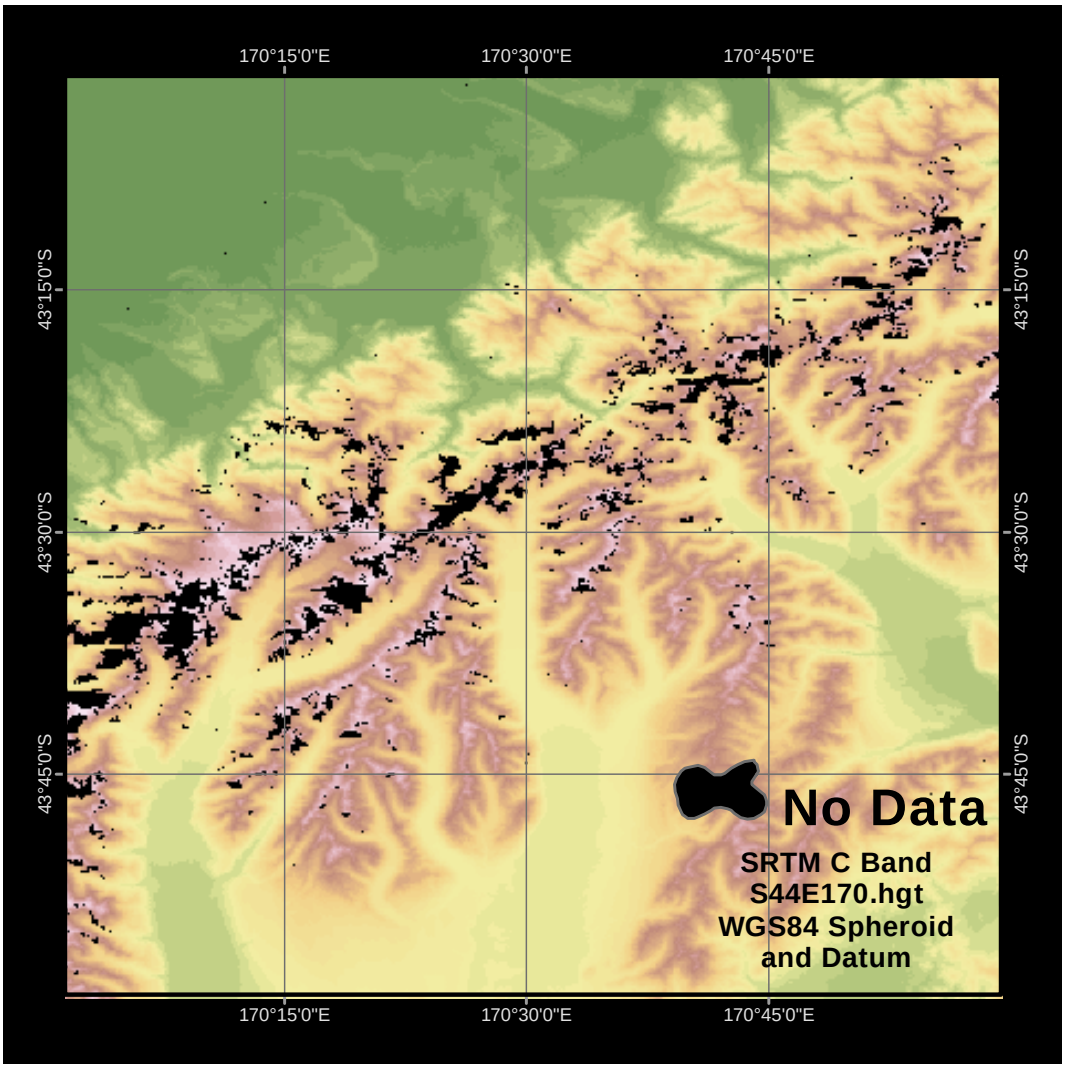

Figure 2.11: Rasterised map of SRTM C band data file S44E170, which covers the Tasman Glacier. Data holes can be seen in black.

Chapter 3

Analysis of Elevation Data

3.1 Introduction

The mass points extracted from the aerial photography and satellite images required filtering to remove errors before they could be compared to the TOPODATA DEM to assess volume change. There is no simple way to filter the data without risking removing points that are truly representative of the surface being modelled. To try to overcome this problem, points were paired with z values from the same locations of the TOPODATA DEM (so that each point had two z values associated with them) and divided into those representing non-glaciated (*rock*) surfaces and those of the Tasman Glacier (*ice*) for each data set. The rock data points were regressed against their TOPODATA z values to determine any vertical bias that the data displayed and to find suitable threshold values for which to filter points from the ice data. This is based on the assumption that rock movement over the area surrounding the glacier has been negligible and that error for ice are of the same magnitude to the errors for rock. The filtered points gave a much more reliable basis for interpolating to produce a regular raster grid which could be averaged by 100 m elevation bands without the influence of point clusters. The end result is a mean elevation value for each 100 m elevation band based on the TOPODATA z values so that they can be directly compared from year to year.

This chapter describes the procedure used to filter and interpolate between the data points so that elevation of the Tasman Glacier surface could be compared from year to year. The results of the analysis are presented and discussed in Section 3.3.

3.2 Data Filtering

Two open source software packages were used for the filtering process, as they provided the tools needed in a way that could be scripted. The processes could be automatically repeated many times with greater tuning at each iteration.

GRASS 6.4: Geographic Resources Analysis Support System was originally developed by the U.S. Army Construction Engineering Research Laboratories to be used for land management and

environmental planning by the U.S. military. Contributions to the package have been made by many different independent people and organisations.

R: a programming language for statistics that was designed to be a freely available version of the *S* statistical programming language. Like GRASS, contributions have been made by many sources.

3.2.1 Pairing with TOPODATA

GRASS was used to pair the data points with those from TOPODATA so that each point had two z values. The points were imported to GRASS using the function `r.in.xyz` with a median criterion. The points were aggregated to a regular grid at the same point spacing (25 m) and geographical origin as the TOPODATA DEM so that each data point lined up exactly with the TOPODATA grid. The median criterion had the effect of smoothing highly variable clusters of points. The points for each data set were paired with their respective TOPODATA elevation.

In the case of SRTM, nearest neighbour was used for pairing as the data were already at a regular spacing of 61×92 m which did not match the TOPODATA DEM. Although this type of pairing is not an ideal situation, it was decided that after averaging over many points in each elevation band, that the error would be close to zero.

3.2.2 Subsetting Non-Glaciated Areas and Tasman Glacier Ice

The points for each data set were split into two subsets; *rock* representing non-glaciated surfaces; and *ice* representing the Tasman Glacier surface. A rock mask was created from the ice and water layers of the TOPODATA vector database and a 50 m buffer applied to ensure that all glaciated surfaces was excluded. The same mask was used for all data sets and is shown in Figure 3.1.

Masks for the Tasman Glacier were manually digitised for each year from orthorectified copies of the images used to extract the elevation data. The same glacier outline as AST2002 was assumed for SRTM as accurate visual interpretation of SRTM was not possible. In the lower part of the glacier, the base of the moraine walls were defined as the glacier boundaries. In the upper part the demarcation was more subjective. In places where the difference between the Tasman Glacier and its tributaries was not naturally defined, the same boundary was used for each year. Small differences in the accumulation area showed the absence of ice or presence of ice from year to year. The upper limit of the SN8595 1986 mask was dictated by the aerial photography coverage for that year.

The most significant differences in glacier ice extent were at the terminus where calving into the Tasman lake has reduced its length.

3.2.3 Filtering Auto-correlated Errors

To find an optimal way of filtering the data points, the rock data subset z values were regressed against their respective TOPODATA z values. Assuming both data sets are correct, the y intercept should be 0 and the slope should be 1. However, as discussed in Section 2.2.3, errors in the data propagate along the ATE search line, which causes auto-correlated errors. By comparing rock to

Figure 3.1: Mask of rock used for all data sets to subset points representing rock. The grey regions are rock and white regions are ice.

rock, errors can be seen which do not correlate well with the rest of the data. To decide on a threshold for removal of these data, points whose z values were farthest from the standard deviation were removed and the regression performed again and the threshold reduced. This was repeated iteratively to remove a small number of points at a time until the r^2 reached 0.99. The final threshold and regression equation was then applied to the ice data. A script was written for the R statistical package to perform the procedure and was tested using the SN8595 data set for which both rock and ice should be the same as TOPODATA. Figure 3.2 shows how the script operates.

3.2.4 Interpolation

To produce a regular raster grid surface DEM, it is necessary to interpolate between the mass points in some way. There are various methods available for interpolating between spatial points, which have slightly different outcomes. The method that is used by photogrammetry software (LPS, ENVI, PCI Geomatica) is delauny triangulation – the same method used to construct triangulated irregular

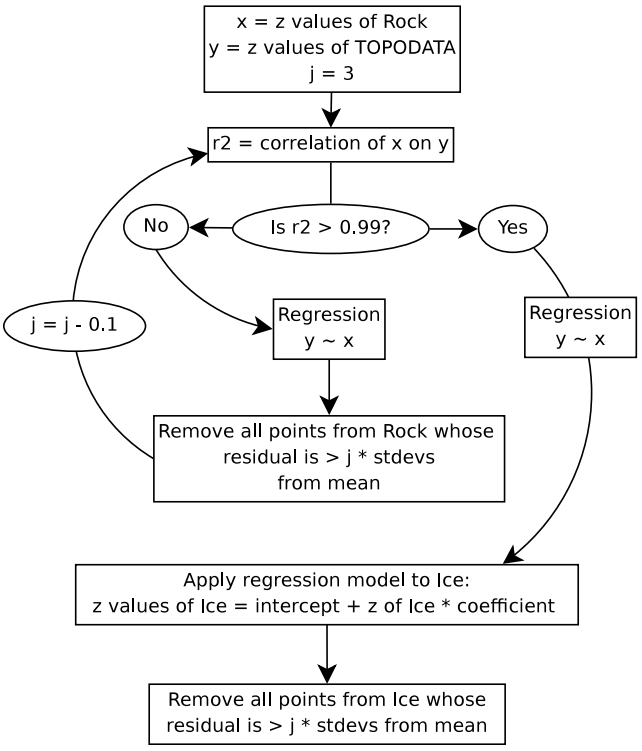

Figure 3.2: Flow diagram showing the procedure used to filter data points. The use of r^2 as the criterion for determining a good fit assumes that the overall hypsometry of the glacier surface remains approximately the same shape, while not necessarily having the same elevation across the glacier. The affine transformation applied to the data using the regression equation compensates for any systematic elevation bias that may be inherent in the data.

networks (TINs). However, this method produces a surface of triangles rather than a smooth surface, and is better suited to vector terrain models that can accurately represent the point spacing where necessary. Because every point is included in the surface, it can also have the effect of amplifying errors, creating large spikes and pits when the data points have not been appropriately filtered before hand.

Regularised spline with tension (RST) is an interpolation method which can reduce the effect of erroneous data points and create a smooth surface that more accurately represents the terrain being modelled. RST interpolation was used on the filtered data to create a uniform surface so that an average elevation could be determined for each 100 m elevation band. The `v.surf.rst` function in GRASS performs the interpolation, with two main options with which to tune the surface character.

Tension changes the stiffness of the surface – a high tension value decreases the influence of each point on the surface between points. *Smoothing* controls the deviation between the given points and the resulting surface – set at 0, the spline passes exactly through each point (Mitasova and Mitas, 1993; Mitasova and Hofierka, 1993).

Quadtree segmentation breaks the data down into segments and the `-t` flag scales the tensioning parameter for each quadtree segment according to the distribution of points. Smoothing was set at 1 and the `-t` flag was used for all data sets. The tension parameters used for each data set are given in Table 3.1.

RST was performed on the elevation values for points derived using ATE as well as their paired TOPODATA values resulting in two interpolated surfaces for each year. An error surface was then obtained to explore the quality of the interpolation process and used to correct the ATE surface using the equation

$$z_c = z_s - (z_{ts} - z_t) \tag{3.1}$$

where z_c is the corrected ATE RST surface, z_s is the uncorrected ATE RST surface , z_{ts} is the TOPODATA RST surface and z_t is the original TOPODATA surface.

Table 3.1: RST tension parameter used for each data set.

Data set	Tension
SN1580	15
SN8595	12
AST2002	7
AST2006	7

3.3 Elevation Change Analysis

The 1986 SN8595 data set was used to test the quality of the method, as the aerial photography used was the same for this study as was used to create the topographic maps from which the TOPODATA DEM was derived. The results of the 1986 data are therefore presented first, followed by 1965, 2000, 2002 and 2006 respectively.

3.3.1 Verification of 1986 Topography Data

Figures 3.3a and 3.3b show scatter plots of rock and ice against TOPODATA for SN8595 and Figure 3.3 show the distributions of their deviations. It can be seen that the kurtosis of the data is very high with a small number of extreme deviations from the mean. Some error propagation can be seen in the ice data set in Figure 3.3b as straight lines of points deviating from the regression line. The data becomes much more scattered at higher elevations, which might be explained for the rock data

by underestimation of the ATE at the top of peaks as the points are more spread out under the $y = 1$ line. The scattering at high elevations on ice is likely to be due to the saturation of the photographs in the upper part of the glacier causing bad matches in the ATE process. It is doubtful whether the TOPODATA DEM is accurate in this area either, making comparison between the two unreliable above around 1900 m.

Summary statistics of the data sets are shown in Table 3.2. The mean of the differences before filtering was reasonably good for rock at -3.851 m. However, the mean for ice was much less so at -9.624 m. Figures 3.5 and 3.6 show the data after the filter was been applied, where $j = 1$, ie. every point with a deviation from the mean of greater than one standard deviation was removed. The kurtosis was significantly reduced and the mean difference for rock reduced to zero. RST improved the mean of the ice to -3.4, some of which can be explained by the different lake extents for SN8595 and TOPODATA.

Table 3.2: Summary statistics for deviations from TOPODATA for SN8595 data points.

Statistic	Before Filtering		After Filtering		After RST
	Rock	Ice	Rock	Ice	Ice
Mean	−3.9	−9.6	0	−7.6	−3.4
Median	−3.6	−8.2	−3.5	−7.5	−2.9
Stdev	100.6	24.9	59.4	10.8	16.0
Min	−756.4	−379.6	−120.5	−33.1	−79.7
Max	613.8	247.7	115.6	16.7	53.6
No. of Points	85818	20232	63171	17265	77249

Figure 3.7a shows the average elevation difference from TOPODATA for each 100 m elevation band for rock and Figure 3.7b shows the same for ice. Both had the same general trend but stay within 10 m of the mean up until around 2300 m, where they quickly trend downwards.

Overall, the data for SN8595 show a reasonable fit to TOPODATA after the filtering has been applied. The fact that the mean rock elevation is zero suggests that the method works well.

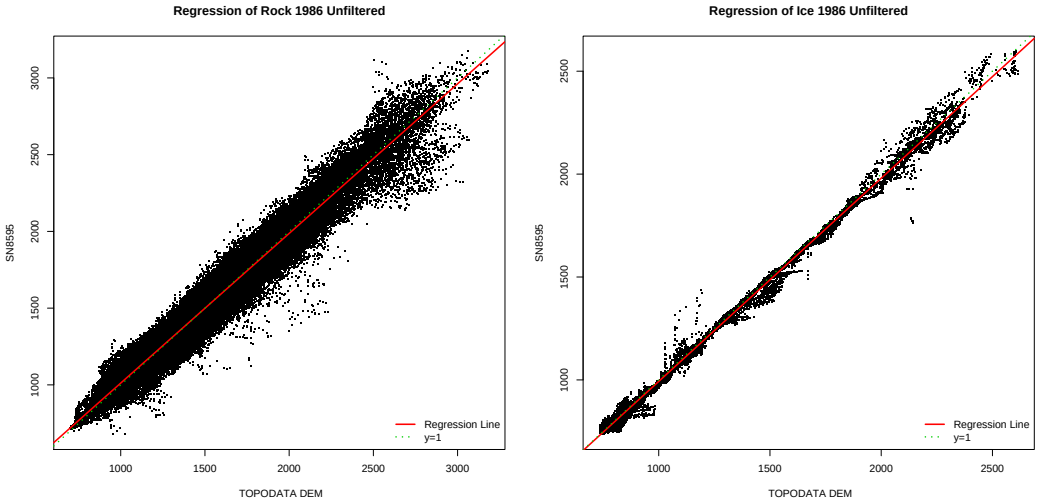

(a) Rock (b) Ice

Figure 3.3: TOPODATA elevations and SN8595 elevations for rock and ice 1986 with regression line before filtering.

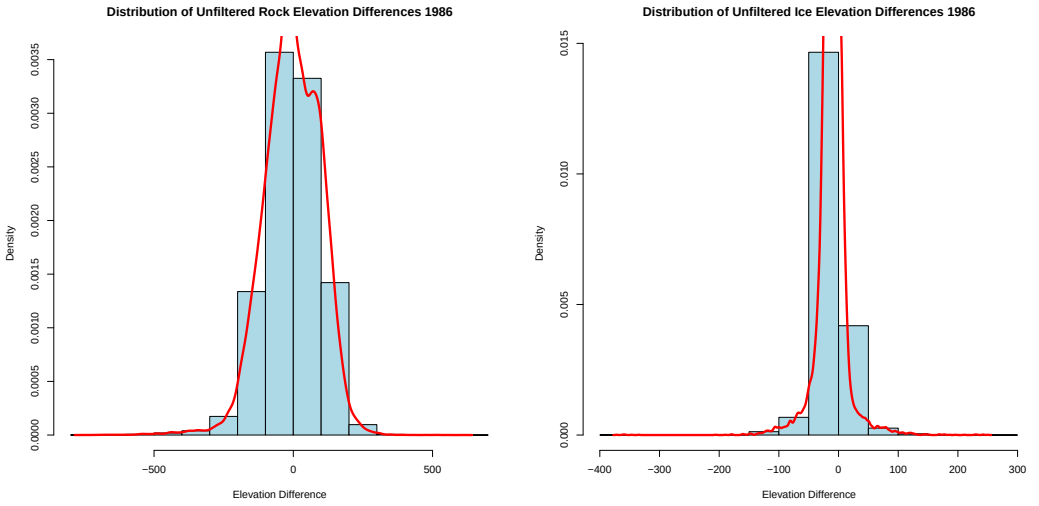

(a) Rock (b) Ice

Figure 3.4: Distribution of differences for rock and ice 1986 before filtering.

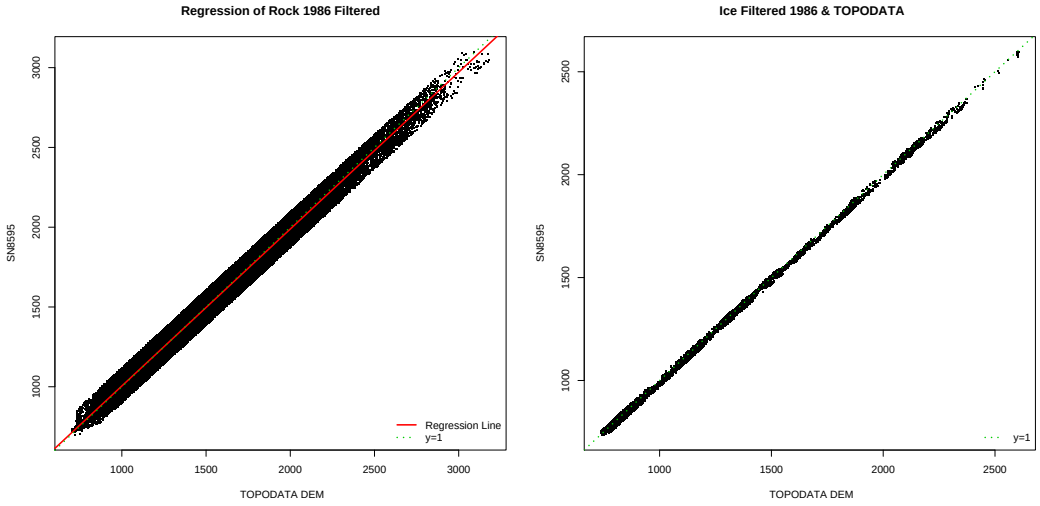

(a) Rock (b) Ice

Figure 3.5: TOPODATA elevations and SN8595 elevations for rock and ice 1986 after filtering.

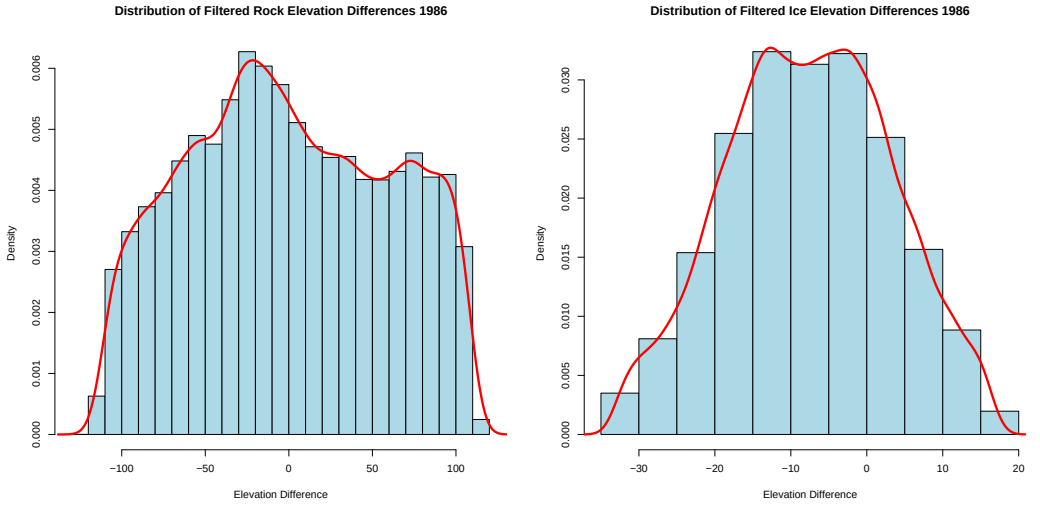

(a) Rock (b) Ice

Figure 3.6: Distribution of differences for rock and ice 1986 after filtering.

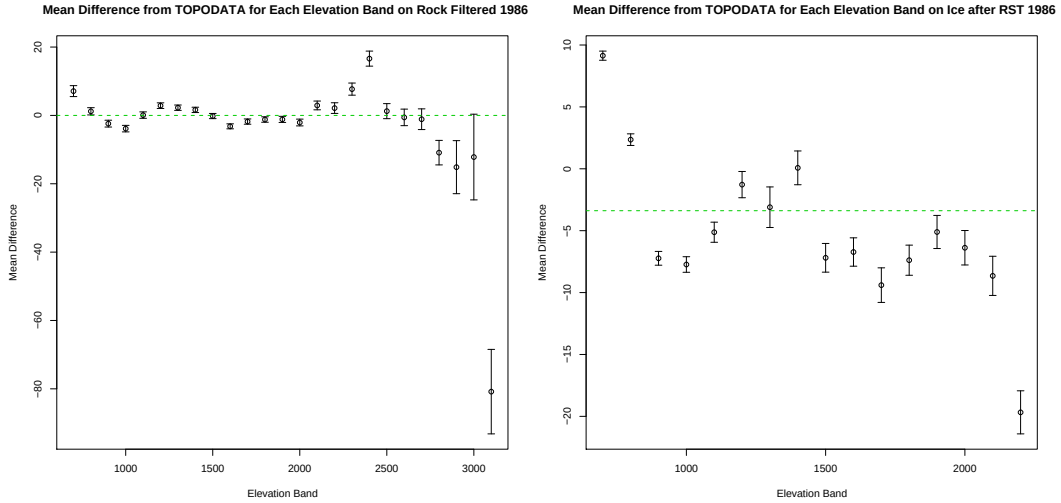

(a) Rock (b) Ice

Figure 3.7: Deviations from TOPODATA averaged over 100 m elevation bands for 1986. Dotted line shows total average. Error bars are 95% confidence intervals.Note the scale differences on the axes. All of the data for rock are shown while only those up to the 2300 m elevation contour for ice is shown, as the data are incomplete past this elevation.

3.3.2 Elevation Change 1986 – 1965

A similar distribution can be seen for SN1580 as seen in SN8595 (Figures 3.8 and 3.9). However the kurtosis is much more extreme with the minimum and maximum difference for rock being -1418 and 743.1 respectively (Table 3.3). The data are extremely scattered, most significantly in the upper part of the glacier, which probably also reflect the high number of data points. However, the high number of points means a more reliable RST surface could be obtained.

After filtering, the data improve significantly as can be seen in Figures 3.10 and 3.11. However, the two peaks in the ice data (Figure 3.11b) become more evident, the reason for which is unknown.

After RST, the mean ice elevations droped to a more reasonable level. The greater concentration of points on the lower glacier, where the drawdown between 1965 and 1986 is expected to be in the order of around 100 m (Figure 1.10), appear to have had a significant effect on the mean which was corrected with RST.

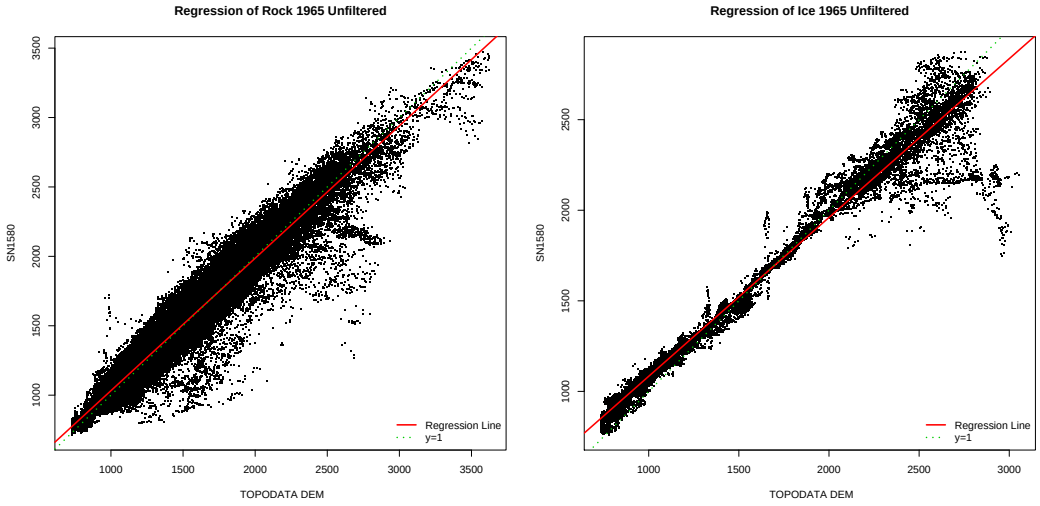

(a) Rock (b) Ice

Figure 3.8: TOPODATA elevations and SN1580 elevations for rock and ice 1965 before filtering.

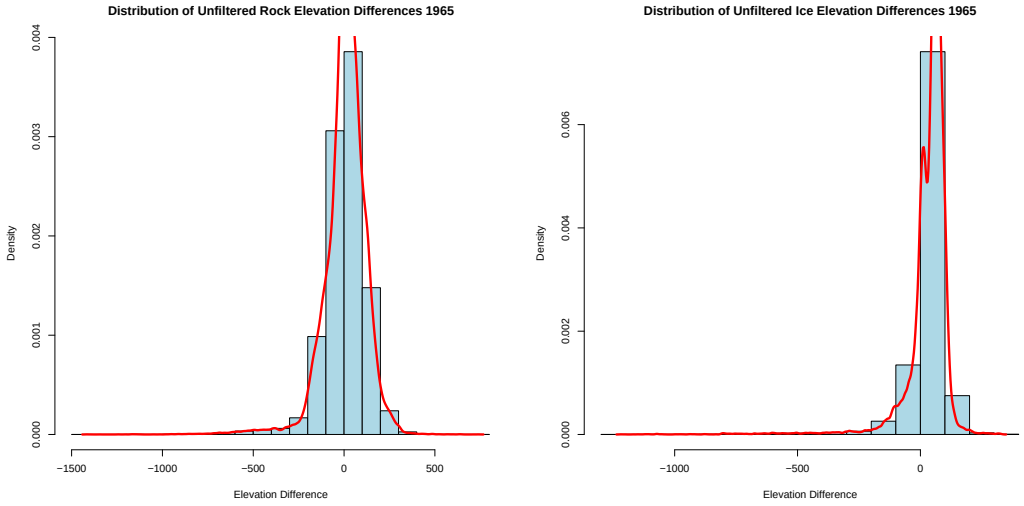

(a) Rock (b) Ice

Figure 3.9: Distribution of differences for rock and ice 1965 before filtering.

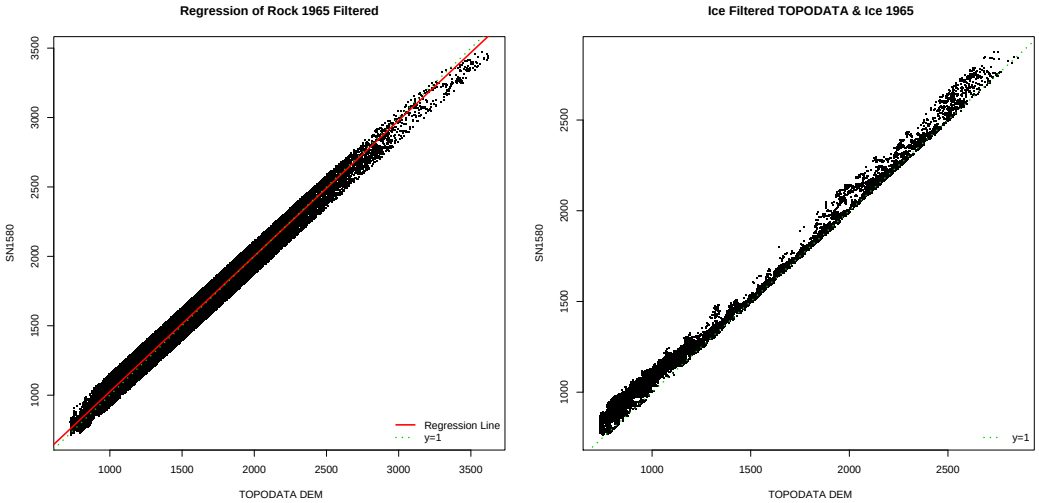

(a) Rock (b) Ice

Figure 3.10: TOPODATA elevations and SN1580 elevations for rock and ice 1965 after filtering.

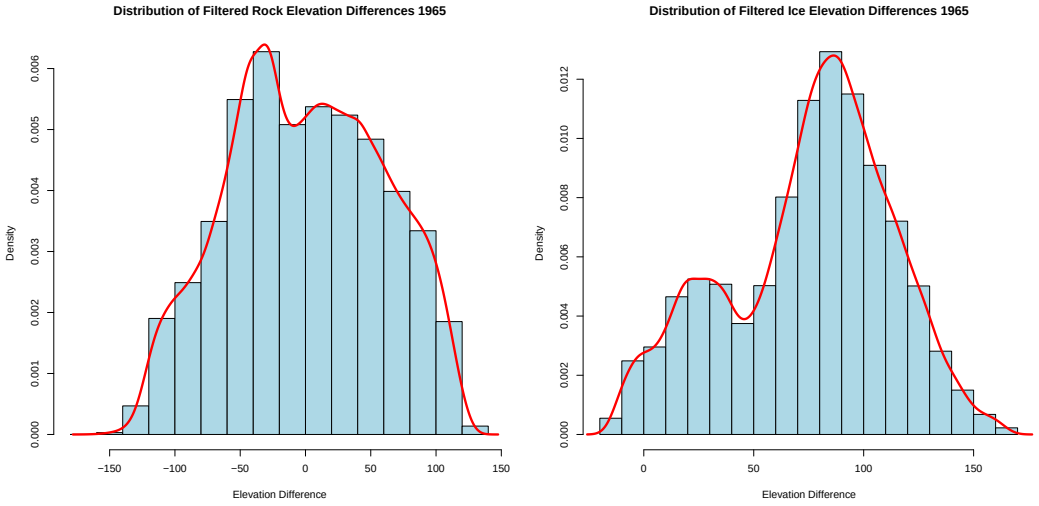

(a) Rock (b) Ice

Figure 3.11: Distribution of differences for rock and ice 1965 after filtering.

Table 3.3: Summary statistics for deviations from TOPODATA for SN1580 data points.

Statistic	Before Filtering		After Filtering		After RST
	Rock	Ice	Rock	Ice	Ice
Mean	6.3	50.8	0	75.3	59.4
Median	13.8	75.4	−0.9	80.8	68.6
Stdev	119.9	98.9	59.3	37.4	50.3
Min	−1418.0	−1214.0	−161.4	−13.6	−86.6
Max	743.1	332.0	130.8	164.5	246.5
No. Points	104565	45380	80475	39389	93578

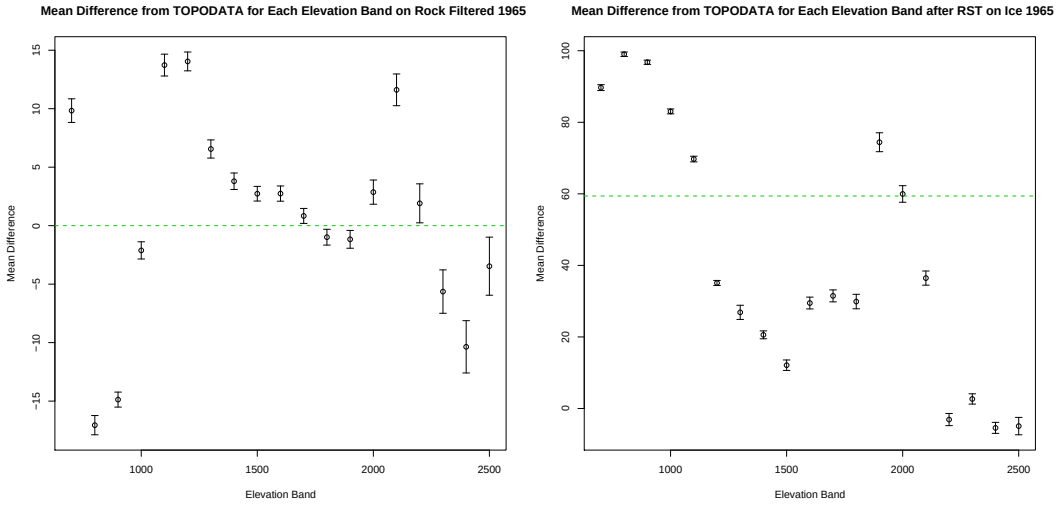

(a) Rock (b) Ice

Figure 3.12: Deviations from TOPODATA averaged over 100 m elevation bands for 1965. Green line shows total average. Error bars are 95% confidence intervals.

3.3.3 Elevation Change 1986 – 2000

SRTM is the only data set that was not extracted using photogrammetric techniques. Several lines of auto-correlated errors could clearly be seen in the unfiltered rock data (Figure 3.13a). These errors were not seen in the ice data (Figure 3.13b). The unfiltered SRTM data is influenced by a very small number of correlated outliers as seen in Figures 3.14a and 3.13a. The fit of the ice data was very good before filtering, showing a fairly normal error distribution (Figure 3.14). The filter only removed just over 100 points in each subset (Table 3.4) and the data still retain their error distribution trends (Figure 3.16).

An interesting feature of Figure 3.15 is the high correlation of the ice data between around 1300 and 1900 m, which coincides with the region of exposed white ice with no supraglacial debris or snow. This feature of the data suggests that there has been little change in that part of the glacier between 1985 and 2000. Figure 3.17a does not show an exact linear relationship with rock either, a trend which is also evident with the other data sets. Berthier et al. (2006) describe a bias in SRTM of up to -10 m being related to elevation. However, this will have been removed after the regression equation was applied. Van Looy et al. (2006) describe a bias of SRTM being related to steepness of terrain, which may be more likely in this case, although the relationship may be more complex.

The overall trend of the SRTM data that can be seen in Figure 3.17 is similar to that seen in the other data sets, albeit with a smoother curve, which suggests that the variances from the means are not unreliable.

Table 3.4: Summary statistics for deviations from TOPODATA for SRTM data points.

Statistic	Before Filtering		After Filtering	
	Rock	Ice	Rock	Ice
Mean	-1.3	-7.3	0	-6.6
Median	1.0	-4.9	-2.3	-4.7
Stdev	100.7	15.9	30.0	13.8
Min	-2989.0	-129.6	-280.4	-50.9
Max	867.0	82.4	167.8	40.9
No. Points	51544	7480	51417	7337

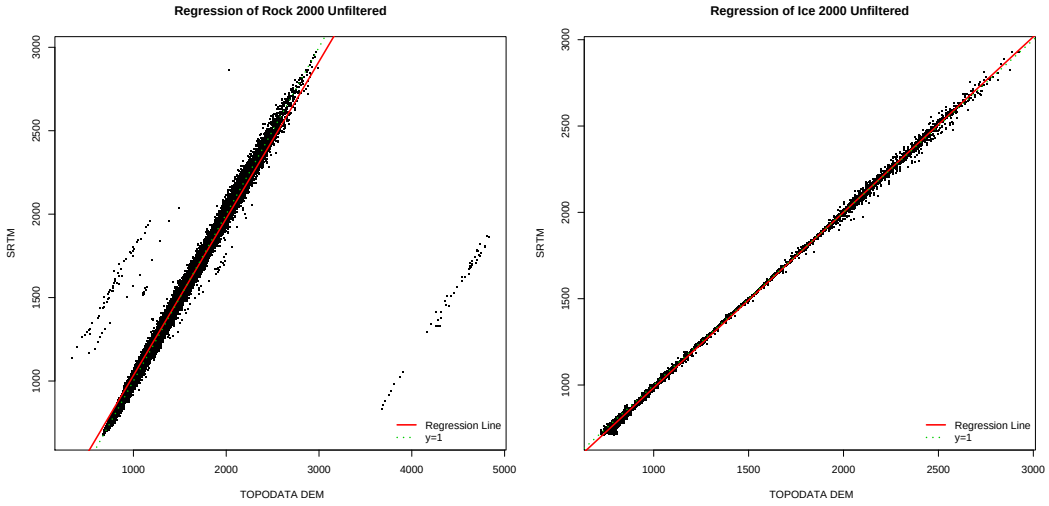

(a) Rock (b) Ice

Figure 3.13: TOPODATA elevations and SRTM elevations for rock and ice 2000 before filtering.

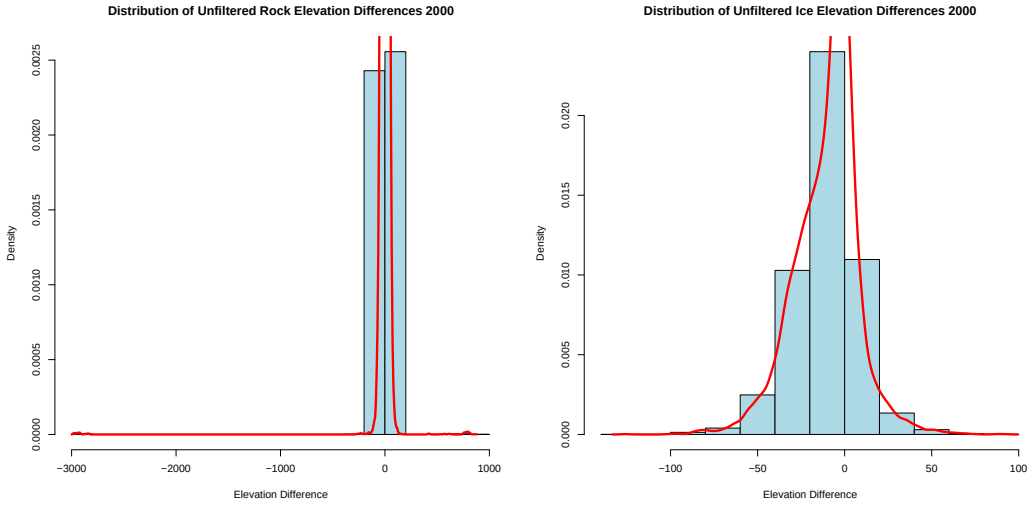

(a) Rock (b) Ice

Figure 3.14: Distribution of differences for rock and ice 2000 before filtering.

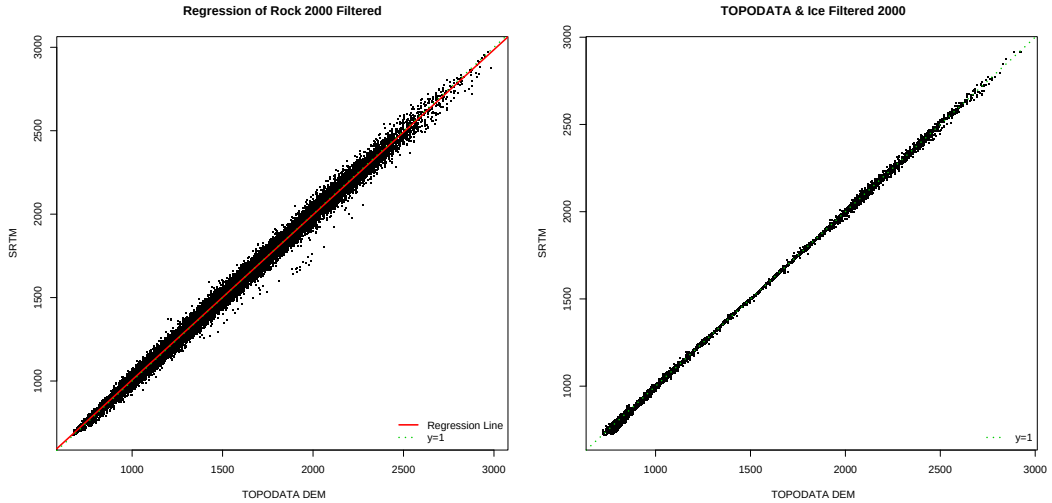

(a) Rock (b) Ice

Figure 3.15: TOPODATA elevations and SRTM elevations for rock and ice 2000 after filtering.

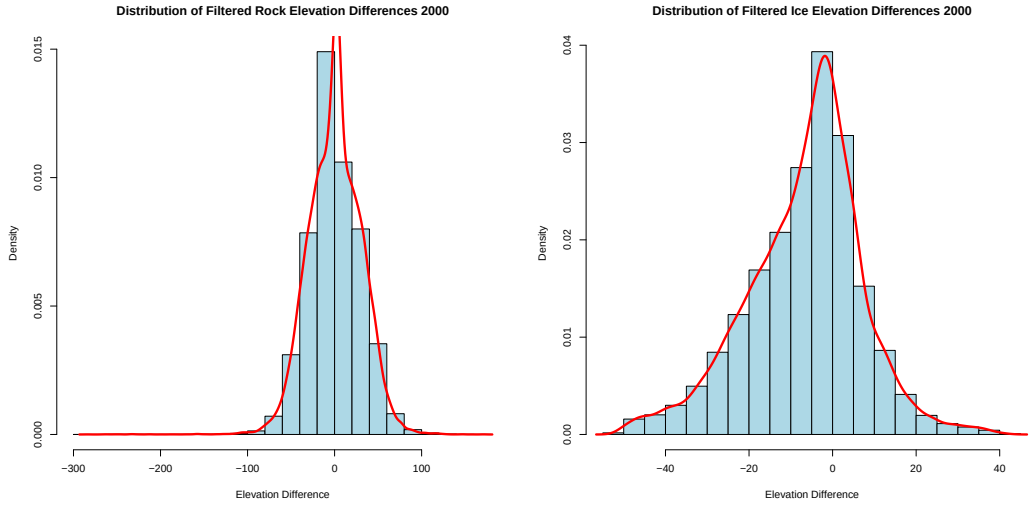

(a) Rock (b) Ice

Figure 3.16: Distribution of differences for rock and ice 2000 after filtering.

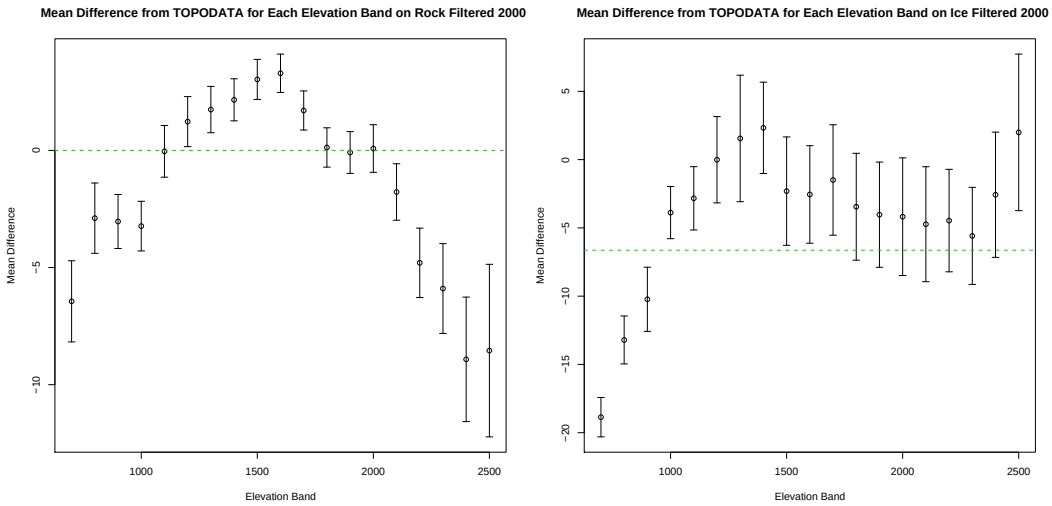

(a) Rock (b) Ice

Figure 3.17: Deviations from TOPODATA averaged over 100 m elevation bands for 2000. Green line shows total average. Error bars are 95% confidence intervals.

3.3.4 Elevation Change 1986 – 2002

The results from the ASTER data were less convincing than for the other data. The summary statistics in Table 3.5 show that the overall response might be reasonable. Figure 3.18 show overall good correlation in the data with only a few outliers scattered about. The error distributions were near normal (Figures 3.19 and 3.21) and filtering did not significantly affect the look of the data (Figure 3.20). However the low point density in the lower part of the glacier below around 1100 m means that below that altitude the data are questionable. Figure 3.22a shows a similar trend to the other rock data subsets, whereas Figure 3.22b does not show much of a trend at all.

Table 3.5: Summary statistics for deviations from TOPODATA for AST2002 data points.

Statistic	Before Filtering		After Filtering		After RST
	Rock	Ice	Rock	Ice	Ice
Mean	1.5	−22.5	0	−23.3	−17.2
Median	−0.7	−22.2	2.6	−22.3	−19.5
Stdev	72.7	40.9	60.8	25.8	33.1
Min	−395.4	−253.2	−142.2	−95.8	−156.0
Max	1476.0	619.1	141.2	51.350	169.2
No. Points	45024	7183	42937	6631	77832

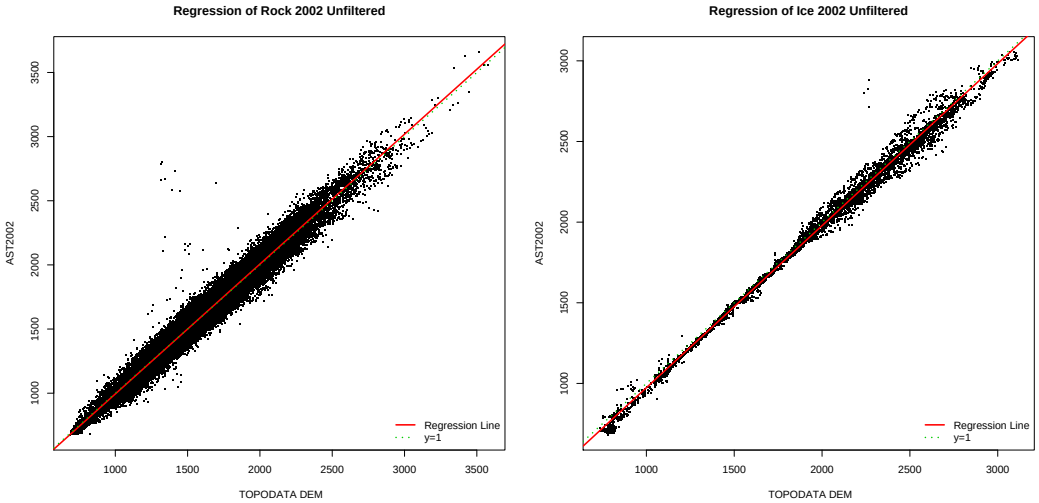

(a) Rock (b) Ice

Figure 3.18: TOPODATA elevations and AST2002 elevations for rock and ice 2002 before filtering.

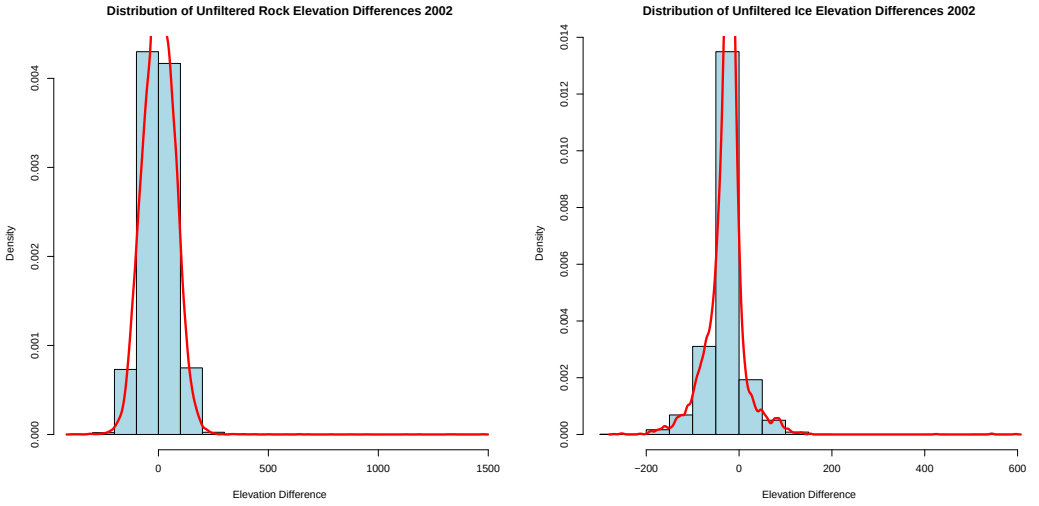

(a) Rock (b) Ice

Figure 3.19: Distribution of differences for rock and ice 2002 before filtering.

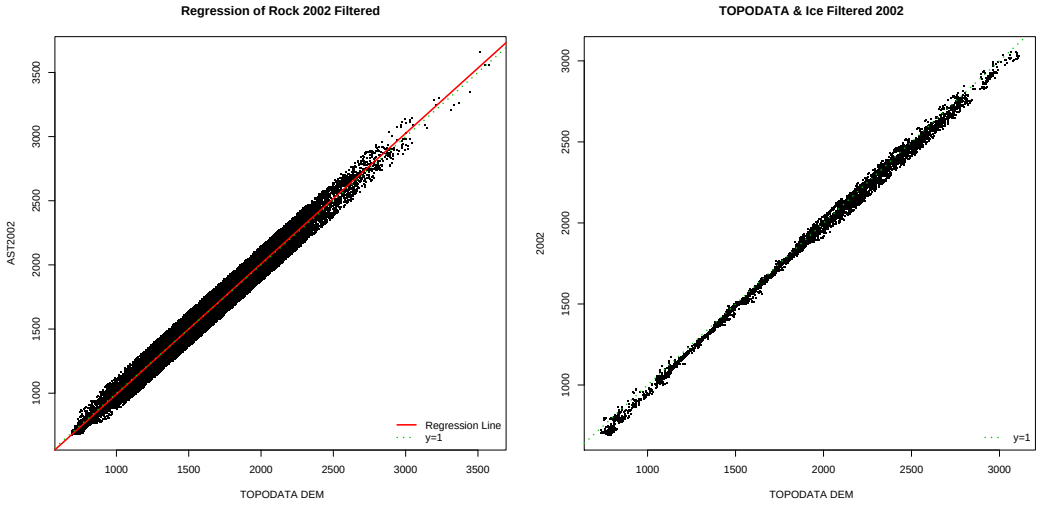

(a) Rock (b) Ice

Figure 3.20: TOPODATA elevations and AST2002 elevations for rock and ice 2002 after filtering.

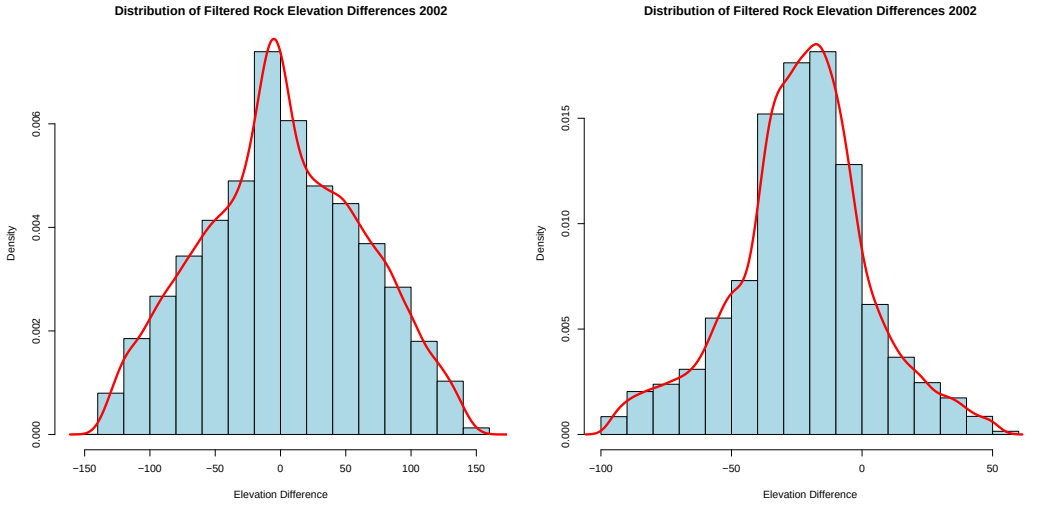

(a) Rock (b) Ice

Figure 3.21: Distribution of differences for rock and ice 2002 after filtering.

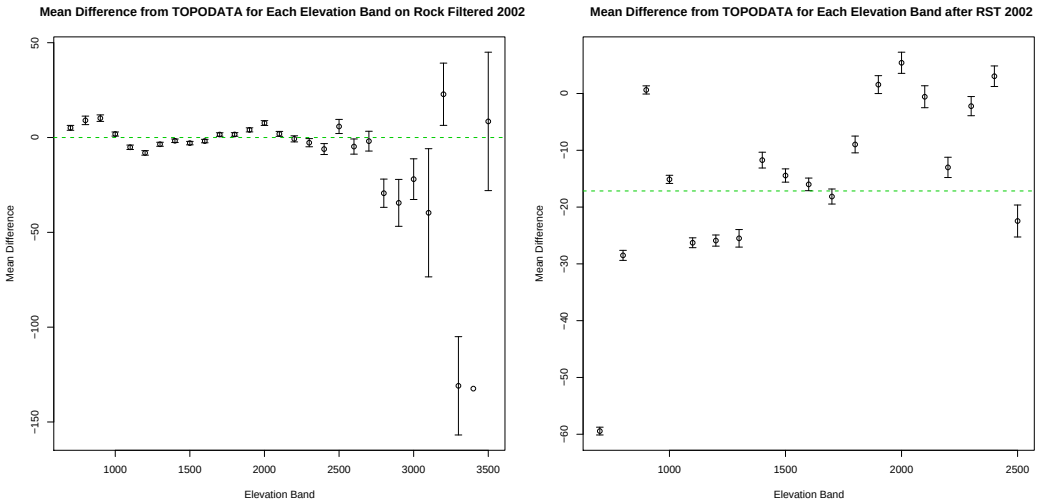

(a) Rock (b) Ice

Figure 3.22: Deviations from TOPODATA averaged over 100 m elevation bands for 2002. Green line shows total average. Error bars are 95% confidence intervals.

3.3.5 Elevation Change 1986 – AST2006

These data show nearly the same error distributions as AST2002 both before (Figures 3.23 and 3.24) and after the filter has been applied (Figures 3.25 and 3.26). The mean differences for rock in Figure 3.27a are almost identical to the AST2002 data set. The similarities are not reflected in the ice data (Figure 3.27b), which after RST shows a overall mean change in elevation of $+1.6$ m (Table 3.6). However, the mean elevation changes appear to be auto-correlated, which suggests that they may indicative of the true trend of the glacier. The results contradict the directly observed thickness change in the lower part of the glacier (Figures 1.10 and 1.11). This discrepancy is likely to be due to poor data quality in that part of the glacier, which is reflected by the high RMSE of the ATE process for the 2006 data (Table 2.4).

Table 3.6: Summary statistics for deviations from TOPODATA for AST2006 data points.

Statistic	Before Filtering		After Filtering		After RST
	Rock	Ice	Rock	Ice	Ice
Mean	9.2	-25.5	0	-12.9	1.6
Median	12.0	-9.2	1.1	-5.3	0.2
Stdev	82.0	56.2	58.9	32.7	52.3
Min	-520.3	-295.2	-140.9	-99.0	-237.8
Max	1198.0	685.7	139.9	80.9	225.4
No. Points	50596	6322	48334	5512	77697

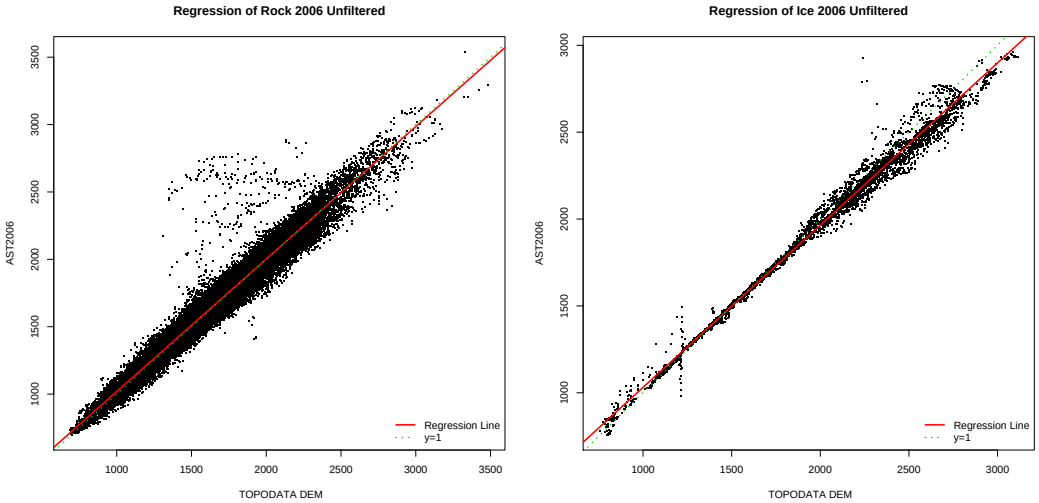

(a) Rock (b) Ice

Figure 3.23: TOPODATA elevations and AST2006 elevations for rock and ice 2006 before filtering.

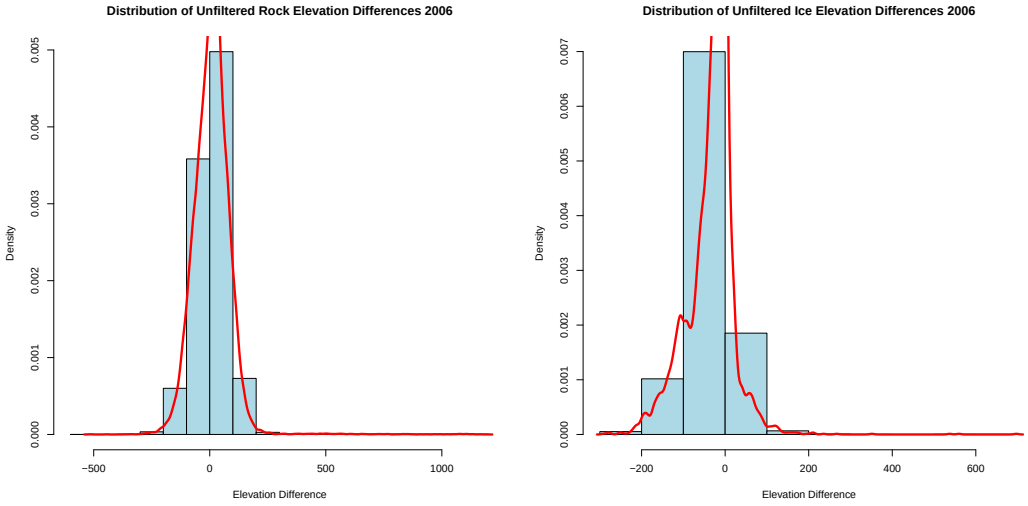

(a) Rock (b) Ice

Figure 3.24: Distribution of differences for rock and ice 2006 before filtering.

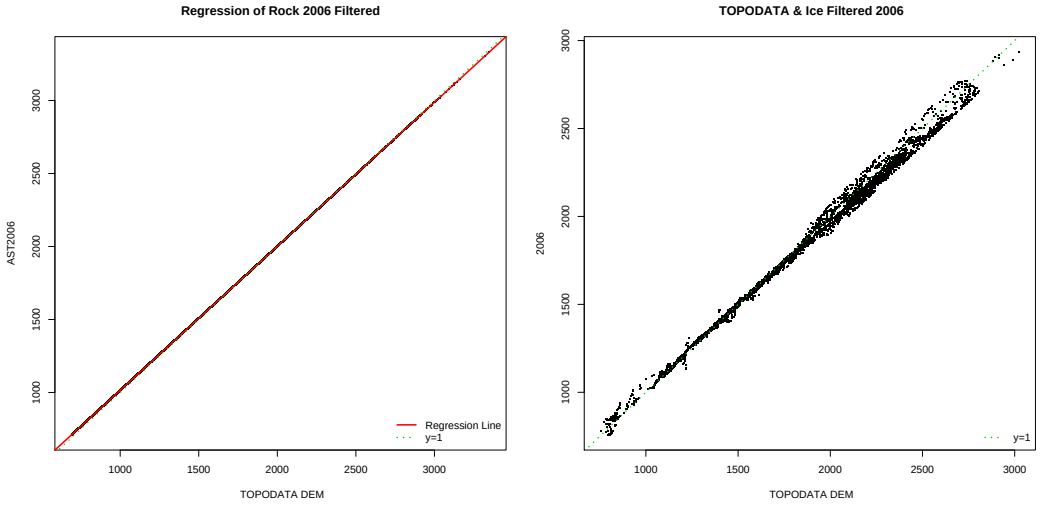

(a) Rock (b) Ice

Figure 3.25: TOPODATA elevations and AST2006 elevations for rock and ice 2006 after filtering.

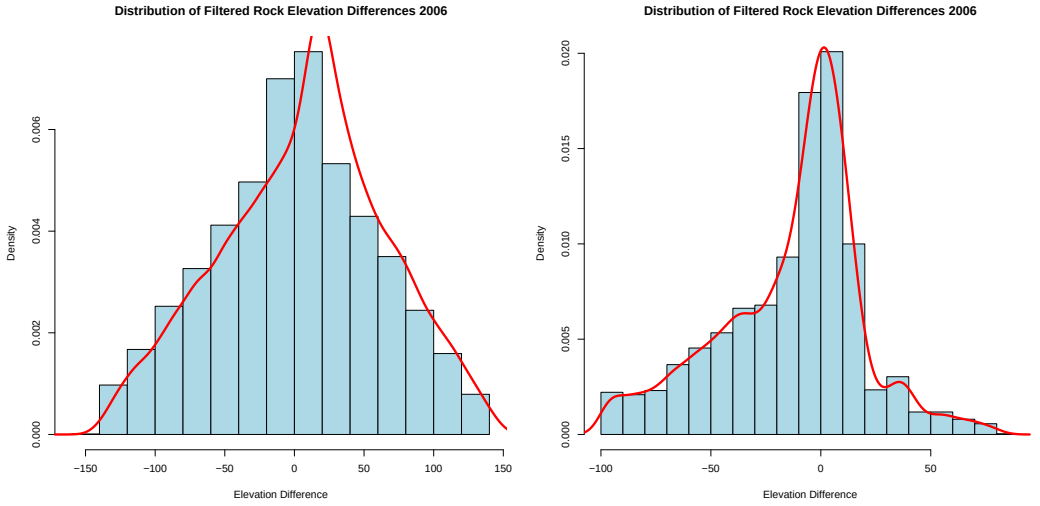

(a) Rock (b) Ice

Figure 3.26: Distribution of differences for rock and ice 2006 after filtering.

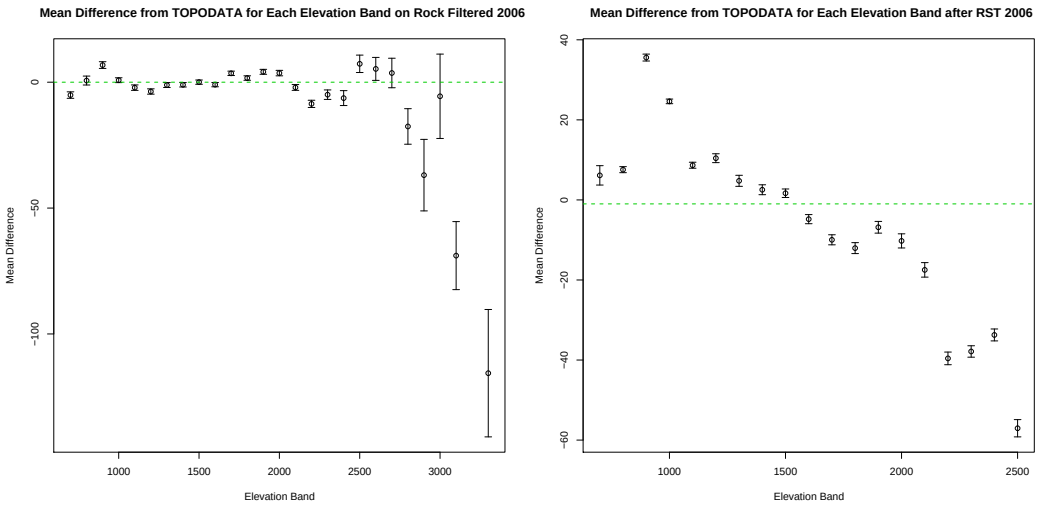

(a) Rock (b) Ice

Figure 3.27: Deviations from TOPODATA averaged over 100 m elevation bands for 2006. Green line shows total average. Error bars are 95% confidence intervals.

3.4 Volume Change of the Tasman Glacier

Figure 3.28 shows the total mean elevation over each elevation band for all years and Figure 3.29 shows the mean differences normalised to the SN1580 1965 data. The correlation between the data set appears to fairly good, apart from the lower elevations of the AST2006 data. An increase in volume in the top elevation bands may not be unexpected considering the quantity and temporal variability of snow fall in the neve.

Volume change is calculated using the equation

$$\Delta V = \sum_{i=1}^{n} A_1 \Delta z_i \tag{3.2}$$

where i is elevation band, A is area of elevation band and Δz_i is change in elevation for that elevation band. AST2006 is not used for comparison due to its apparent unreliability. Using the method presented here, the total volume change of the Tasman Glacier between 1965 and 2006 is 3.4 km^3 or 0.092km^3 per year, which is around 6% of the total estimated ice volume in New Zealand (Chinn, 1991). This figure is likely to be greater when the expansion of the Tasman Lake is taken into account.

3.4.1 Comparison with End of Summer Snowline Survey

Chinn et al. (2007) used the EOSS record to estimate volume change of glaciers in New Zealand, including the Tasman Glacier. A single value for the EOSS was calculated for the whole Southern

Alps and then the EOSS values for each glacier were in turn regressed against the yearly mean values. The y intercept provided the equilibrium line altitude (ELA) for each glacier. For each annual deviation from the ELA in m, the respective annual ablation and accumulation areas were read off the glacier area-altitude curve giving the accumulation area ratio (AAR). The mean mass balances were then obtained from the mass balance gradient – assumed to be 7.1 mm m^{-1} and 12.5 mm m^{-1} for the accumulation and ablation areas respectively for the eastern glaciers (including Tasman). Volume change for each glacier was then calculated as

$$\Delta V = \frac{A_{acc}(H_{max} - EOSS)\frac{\delta b}{\delta z_{acc}}}{2} - \frac{A_{abl}(H_{min} - EOSS)\frac{\delta b}{\delta z_{abl}}}{2} \tag{3.3}$$

where A_{acc} is accumulation area, H_{max} is maximum altitude, $\delta b/\delta z_{acc}$ is the balance gradient for the accumulation area and *abl* is ablation. This formula does not take into account draw down and terminus lake growth, which are significant factors for the Tasman Glacier. These parameters had to measured by comparing topographic maps, aerial photographs and from bathymetry measurements of the lake. This method gives a total volume loss of the Tasman Glacier between 1977 and 2005 of 1.78 km^3 or 0.064km^3 per year.

3.4.2 Methodological Problems

The overall trend between years of glacier elevation change is relatively similar, although there is some obvious systematic non-linear distortion that can be seen in the rock subsets. The cause of this distortion is likely to be due to the quality of the GCPs. Every effort was made to collect GCPs in the field for the SN8595 photography, but was limited by the rapidly changing landscape surrounding the glacier and accessibility of the area. This may not be such an issue for the ASTER data due to its relatively low spatial resolution.

The quality of the SN8595 photography was not ideal with large areas of ice being completely white, which prevented feature correlation in those areas. This is a problem that the SN1580 photography did not suffer from to the same degree. The ASTER data had the same problem on the debris covered part of the glacier, where the only points extracted were manually digitised tie points.

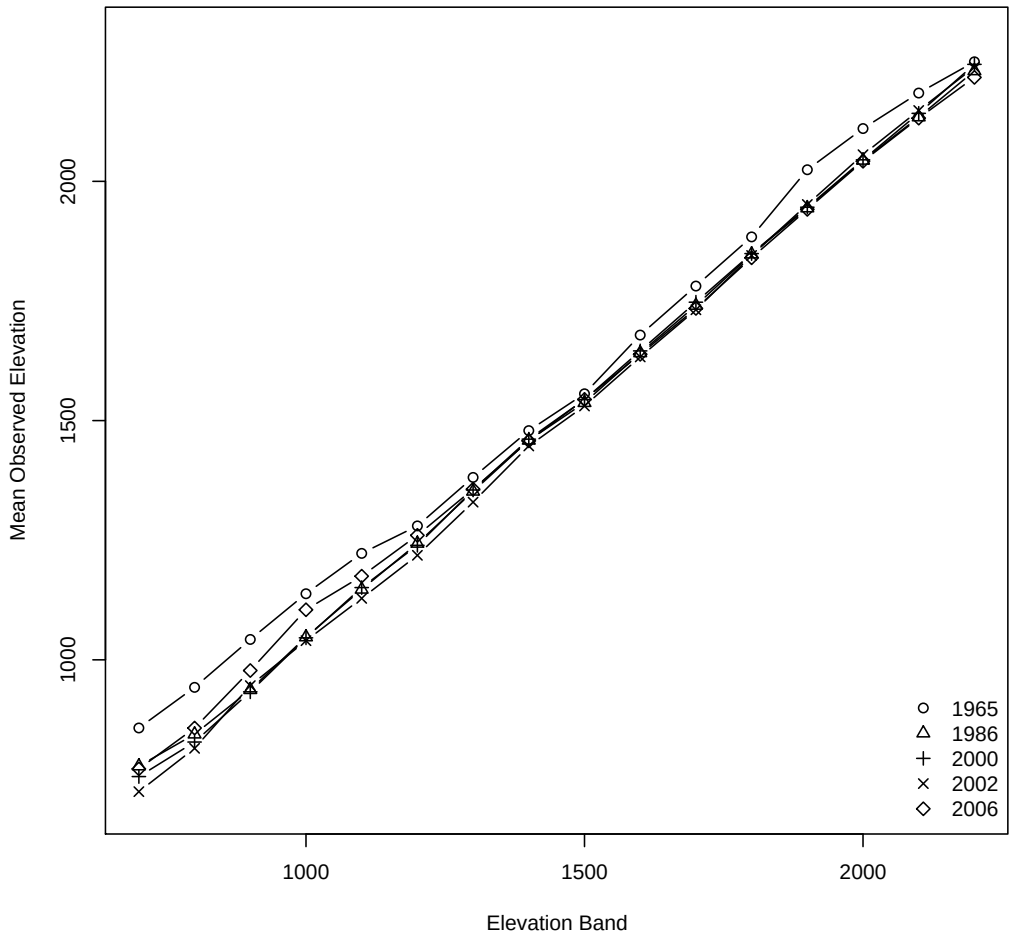

Figure 3.28: Mean elevation for each elevation band for all years.

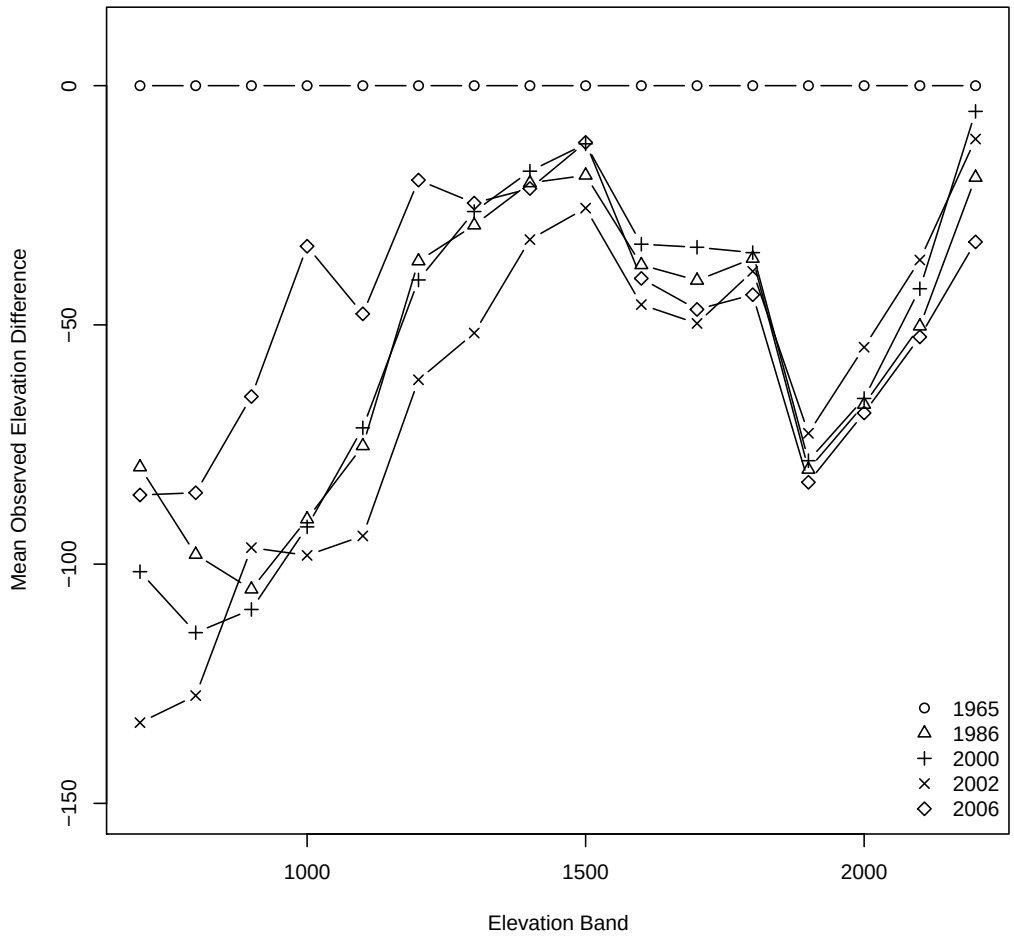

Figure 3.29: Mean elevation change for each elevation band normalised to the SN1580 1965 data.

Chapter 4

Conclusions

4.1 Summary

This study explored the possibility of measuring volume change of the Tasman Glacier using remotely sensed data. Aerial photography and ASTER imagery were converted into three dimensional point clouds using digital photogrammetry techniques. Elevation data from SRTM was also acquired.

Data were compared to the existing TOPODATA DEM for their reliability. While the quality of the SRTM data is very high, there is a second order distortion present in the data that is evident over elevation differences. However, the overall mean difference of the SRTM rock from TOPODATA is close to zero.

The quality of the data extracted from the aerial photography was very good on rock and debris covered ice, but poor on snow. The data extracted from ASTER was much more reliable on snow in the upper glacier than the aerial photography, but was very poor in the lower debris covered region of the glacier.

Overall, a trend could be seen in the data between dates. Better image correlation might be achieved if the aerial photography was scanned from the negatives using a photogrammetric scanner. With a set of about 30 good quality GCPs for these photographs, it may be possible to construct a block of highly accurate stereo models for the region from which subsequent data sets may be registered to. However, it is questionable whether it would be possible to obtain such GCPs given the changing terrain of the region.

The spatial resolution of ASTER makes high temporal resolution monitoring of volume change unlikely for the New Zealand glaciers. The infrequency of aerial photography, the high cost and vast time involved in extracting good quality elevation data from aerial photography makes it impractical for monitoring glacier volume change remotely. However, SRTM and other radar sensors may provide a better solution, as these types of data do not rely on point matching and measuring image geometry.

4.2 Extensibility of the Methods

To test the method on a smaller glacier, three sets of aerial photography and two satellite images were obtained of the Brewster Glacier in Mount Aspiring National Park. However, no reliable elevation data was able to be extracted from any of these sets of imagery. It is therefore unlikely that the method could be scaled to measure the volume change of smaller glaciers. Currently the EOSS survey works well for these glaciers.

Small scale radar data with high vertical precision may provide the best means for monitoring glacier volume change over the whole Southern Alps.

4.3 Further Work

It is recommended that a more comprehensive ground survey be conducted covering three aerial photographs. The photography should cover an area comprising a mountain ridge, slope, the moraine wall and a cross-section of the glacier. At the time of writing, the Aoraki region is scheduled to be re-photographed using modern digital photogrammetric camera equipment. GCP should be collected as close as possible to the time of acquisition of this aerial photography. This smaller, more comprehensive survey will enable a better understanding of the variables causing distortion, as well as determining optimal settings for the ATE process.

References

Aizen, V. B., Kuzmichenok, V. A., Surazakov, A. B. and Aizen, E. M. (2007). Glacier changes in the Tien Shan as determined from topographic and remotely sensed data, *Global and Planetary Change* **56**: 328–340.

Anderton, P. W. (1975). Tasman Glacier, *Hydrological Research: Annual Report 33*, National Water and Soil Conservation Organisation.

Anderton, P. W. and Chinn, T. J. (1978). Ivory Glacier, New Zealand, an I.H.D. representative basin study, *Journal of Glaciology* **20**(82): 67–84.

Andrews, J. T. (2006). Glaciers, oceans, atmosphere and climate, *in* P. G. Knight (ed.), *Glacier Science and Environmental Change*, Blackwell, Malden, pp. 96–113.

Arendt, A. A., Echelmeyer, K. A., Harrison, W. D., Lingle, C. S. and Valentine, V. B. (2002). Rapid wastage of Alaska glaciers and their contribution to rising sea level, *Science* **297**(5580): 382–386.

Barringer, J. R. F., Pairman, D. and McNeill, S. J. (2002). Development of a high-resolution digital elevation model for New Zealand, *Landcare research contract report: Lc0102/70*, Wellington.

Barry, R. G. (2006). The status of research on glaciers and global glacier recession: a review, *Progress in Physical Geography* **30**(3): 285–306.

Berthier, E., Arnaud, Y., Baratoux, D., Vincent, C. and Rémy, F. (2004). Recent rapid thinning of the "Mer de Glace" Glacier derived from satellite optical images, *Geophysical Research Letters* **31**. L17401.

Berthier, E., Arnaud, Y., Vincent, C. and Rémy, F. (2006). Biases of SRTM in high-mountain areas: Implications for the monitoring of glacier volume changes, *Geophysical Research Letters* **33**. L08502.

Bolch, T., Kamp, U. and Olsenholler, J. (2005). Using ASTER and SRTM DEMs for studying geomorphology and glaciation in high mountain areas, *in* M. Oluić (ed.), *New Strategies for European Remote Sensing*.

Braithwaite, R. J. (1984). Can the mass balance of a glacier be estimated from its equilibrium line altitude?, *Journal of Glaciology* **30**(1006): 364–368.

Brodrick, T. (1894). Ice motion of the Canterbury glaciers, *The New Zealand Alpine Journal* **1**: 307–316.

Brodrick, T. N. (1891a). Map of the Tasman and Murchison Glaciers. No. 60T, Deposited at the Department of Lands and Survey, Christchurch.

Brodrick, T. N. (1891b). Report on the Tasman Glacier, *Appendix to the Journal of the House of Representatives of New Zealand, 1891 session II* **1**(C-1A): 39–43.

Brodrick, T. N. (1906). Glacier Movement, *Appendix to the Journal of the House of Representatives of New Zealand, session II* **1**(C-1A): 16–17.

Burrows, C. J. (2005). *Julius Haast in the Southern Alps*, Canterbury University Press, Christchurch.

Cazenave, A. and Nerem, R. S. (2004). Present-day sea level change: observations and causes, *Reviews of Geophysics* **42**: RG3001 1–20.

Cheng, X., Zhang, Y., E, D., Li, Z. and Shao, Y. (2003). Digital elevation model construction using ASTER stereo VNIR scene in Antarctic in-land ice sheet, *IEEE International Geoscience and Remote Sensing Symposium*, Vol. 5, pp. 3347–3349.

Chinn, T. (1991). Glacier Inventory of New Zealand. Unpublished report of the Institute of Geological and Nuclear Sciences, Dunedin.

Chinn, T. (1995). Glacier fluctuations in the Southern Alps of New Zealand determined from snowline elevations, *Arctic and Alpine Research* **27**(2): 187–198.

Chinn, T. (2001). Distribution of the glacial water resources of New Zealand, *Journal of Hydrology* **40**(2): 139–187.

Chinn, T., Salinger, J., Fitzharris, B. and Willsman, A. (2007). Annual ice volume changes 1976–2005 for the New Zealand Southern Alps, *In Press* .

Dyurgerov, M. (2002). Glacier mass balance and regime: Data of measurements and analysis, Occasional Paper No. 55, Institute of Arctic and Alpine Research, University of Colorado.

Dyurgerov, M. (2003). Mountain and subpolar glaciers show an increase in sensitivity to climate warming and intensification of the water cycle, *Journal of Hydrology* **282**(1-4): 164–176.

Dyurgerov, M. B. and Meier, M. (1997). Mass balance of mountain and subpolar glaciers: A new global assessment for 1961–1990, *Arctic and Alpine Research* **29**(4): 379–391.

Fitzharris, B., Lawson, W. and Owens, I. (1999). Research on glaciers and snow in New Zealand, *Progress in Physical Geography* **23**(4): 469–500.

GCOS (2004). *Implementation Plan for the Global Observing System for Climate in Support of the UNFCCC*, GCOS 92 (WMO/TD no. 1219), Geneva.

Gellatly, A. F. (1985). Historical Records of Glacier Fluctuations in Mt Cook National Park, New Zealand: A Century of Change, *The Geographical Journal* **151**: 86–99.

George, L. A. (2005). *Mass balance and climate interactions at Brewster Glacier, 2004/5*, Master's thesis, Department of Geography, University of Otago, Dunedin.

Gjermundsen, E. F. (2007). *Recent changes in glacier area in the Central Southern Alps of New Zealand*, Master's thesis, Department of Geosciences, University of Oslo.

Goldthwait, R. P. and McKeller, I. C. (1962). New Zealand Glaciology, *Antarctic Research: Geophysical Monograph No. 7*, American Geophysical Union, pp. 209–216.

Gornitz, V., Lebedeff, S. and Hansen, J. (1982). Global sea level trend in the past century, *Science* **215**(4540): 1611–1614.

Griffiths, G. and McSaveney, M. (1983). Distribution of mean annual precipitation across some steep-land regions of New Zealand, *New Zealand Journal of Science* **26**: 197–209.

Grove, J. M. (2004). *Little Ice Ages: Ancient and Modern*, Vol. 1, 2nd edn, Routledge, New York.

Haeberli, W. (2006). Integrated perception of glacier changes: a challenge of historical dimensions, *in* P. G. Knight (ed.), *Glacier Science and Environmental Change*, Blackwell, Malden, pp. 423–430.

Haeberli, W., Cihlar, J. and Barry, R. G. (2000). Glacier monitoring within the Global Climate Observing System, *Annals of Glaciology* **31**: 241–246.

Hochstein, M. P., Claridge, D., Henrys, S. A., Alex, P., Nobes, D. C. and Leary, S. F. (1995). Downwasting of the Tasman Glacier, South Island, New Zealand: changes in the terminus region between 1971 and 1993, *New Zealand Journal of Geology and Geophysics* **38**: 1–16.

Hooke, R. L. (2005). *Principles of Glacier Mechanics*, 2nd edn, Cambridge University Press, Cambridge.

Hubbard, A., Willis, I., Sharp, M., Mair, D., Nienow, P., Hubbard, B. and Blatter, H. (2000). Glacier mass-balance determination by remote sensing and high-resolution modelling, *Journal of Glaciology* **46**(154): 491–498.

IUGG, UNEP and UNESCO (2005). *Fluctuations of Glaciers 1995–2000*, World Glacier Monitoring Service, Paris.

Kääb, A. (2002). Monitoring high-mountain terrain deformation from repeated air- and spaceborne optical data: examples using digital aerial imagery and ASTER data, *ISPRS Journal of Photogrammetry and Remote Sensing* **57**(1-2): 39–52.

Kääb, A., Huggel, C., Paul, F., Wessels, R., Raup, B., Kieffer, H. and Kargel, J. (2002). Glacier monitoring from ASTER imagery: accuracy and applications, *Proceedings of EARSeL-LISSIG-Workshop Observing our Cryosphere from Space*, number 2, Bern.

Kamp, U., Bolch, T. and Olsenholler, J. (2003). DEM Generation from ASTER Satellite Data for Geomorphometric Analysis of Cerro Sillajhuay, Chile/Bolivia, *Proceedings Annual Meeting Imaging and Geospatial Information Society (ASPRS)*, Anchorage, U.S.A.

Keating, T. J., Wolf, P. R. and Scarpace, F. L. (1975). An Improved Method of Digital Image Correlation, *Photogrammetric Engineering and Remote Sensing* **41**(8): 993.

Khalsa, S., Dyurgerov, M., Khromova, T. and Raup, R. (2004). Space-based mapping of glacier changes using ASTER and GIS tools, *IEEE Transactions on Geoscience and Remote Sensing,* **42**(10): 2177–2183.

Kirkbride, M. (1989). *The Influence of Sediment Budget on Geomorphic Activity of the Tasman Glacier, Mount Cook National Park, New Zealand*, PhD thesis, Department of Geology, University of Canterbury.

Kuhn, M. (1984). Mass budget imbalances as a criteria for a climatic classification of glaciers, *Geografiska Annaler* **66A**(3): 229–238.

Larsen, C. F., Motyka, R. J., Arendt, A. A., Echelmeyer, K. A. and Geissler, P. E. (2007). Glacier changes in southeast Alaska and northwest British Columbia and contribution to sea level rise, *Journal of Geophysical Research* **112**: F01007.

Leica (2006). *Leica Photogrammetry Suite Automatic Terrain Extraction*, Leica Geosystems Geospatial Imaging, LLC, Norcross.

Leonard, K. and Fountain, A. G. (2003). Map-based methods for estimating glacier equilibrium-line altitudes, *Journal of Glaciology* **49**(166): 329–336.

Meier, M. (1965). Glaicers and climate, *in* H. Wright and D. Frey (eds), *The Quaternary of the United States*, Princeton University Press, Princeton, pp. 795–805.

Meier, M. (1984). Contribution of small glaciers to global sea level, *Science* **226**(4681): 1418–1421.

Meier, M. and Bahr, D. (1996). Counting glaciers: use of scaling methods to estimate the number and size distribution of the glaciers of the world, *in* S. Colbeck (ed.), *Glaciers, ice sheets and volcanoes: a tribute to Mark F. Meier*, US Army Corps of Engineers, Cold Regions Research and Engineering Laboratory, CRREL Special Report 96-27, pp. 89–94.

Meier, M. F., Dyurgerov, M. B. and McCabe, G. J. (2003). The health of glaciers: recent changes in glacier regime, *Climatic Change* **59**: 123–135.

Meier, M. F., Dyurgerov, M. B., Rick, U. K., O'Neel, S., Pfeffer, W. T., Anderson, R. S., Anderson, S. P. and Glazovsky, A. F. (2007). Glaciers Dominate Eustatic Sea-Level Rise in the 21st Century, *Science Express Reports* **Published online July 19 2007**: 10.1126/science.1143906.

Mitasova, H. and Hofierka, J. (1993). Interpolation by Regularized Spline with Tension: II. Application to Terrain Modeling and Surface Geometry Analysis, *Mathematical Geology* **25**: 657–667.

Mitasova, H. and Mitas, L. (1993). Interpolation by Regularized Spline with Tension: I. Theory and Implementation, *Mathematical Geology* **25**: 641–655.

Muskett, R. R., Lingle, C. S., Sauber, J. M., Rabus, B. T. and Tangborn, W. V. (2008). Acceleration of surface lowering on the tidewater glaciers of Icy Bay, Alaska, U.S.A. from InSAR DEMs and ICESat altimetry, *Earth and Planetary Science Letters* **265**: 345–359.

NASA (2006). *Earth Science Reference Handbook*, National Aeronautics and Space Administration (NASA), Washington, D.C.

National Snow and Ice Data Center (2005). *World glacier inventory*, World Glacier Monitoring Service and National Snow and Ice Data Center/World Data Center for Glaciology, Boulder.

Østrem, G. and Brugman, M. (1991). *Glacier mass-balance measurements. A manual for field and office work*, NHRI Science Report 4, Environment Canada. National Hydrology Research Institue, Saskatoon.

Paterson, W. S. (1994). *The Physics of Glaciers*, 3rd edn, Butterworth-Heinemann, Oxford.

Rignot, E., Echelmeyer, K. and Krabill, W. (2001). Penetration depth of interferometric synthetic-aperture radar signals in snow and ice, *Geophysical Reasearch Letters* **28**(18): 3501–3504.

Rignot, E., Rivera, A. and Casassa, G. (2003). Contribution of the Patagonia icefields of South America to sea level rise, *Science* **302**(5644): 434–438.

Rivera, A. and Casassa, G. (2004). Ice elevation, areal, and frontal changes of glaciers from National Park Torres del Paine, Southern Patagonia Icefield, *Arctic, Antarctic and Alpine Research* **36**(4): 379–389.

Rivera, A., Casassa, G., Bamber, J. and Kääb, A. (2005). Ice-elevation changes of Glaciar Chico, southern Patagonia, using ASTER DEMs, aerial photographs and GPS data, *Journal of Glaciology* **51**(172): 105–112.

Ruddell, A. R. (1995). *Recent Glacier and Climate Change in the New Zealand Alps*, PhD thesis, School of Earth Sciences, University of Melbourne.

Salinger, M. J. (1980). New Zealand climate 1. Precipitation patterns, *Monthly Weather Review* **180**: 1892–1904.

Sapiano, J. J., Harrison, W. D. and Echelmeyer, K. A. (1998). Elevation, volume and terminus changes of nine glaciers in North America, *Journal of Glaciology* **44**(146): 119–135.

Schiefer, E., Menounos, B. and Wheate, R. (2007). Recent volume loss of British Columbian glaciers, Canada, *Geophysical Research Letters* **34**: L16503.

Skinner, B. E. (1964). Measurements of twentieth century ice loss on the Tasman Glacier, New Zealand, *New Zealand Journal of Geology and Geophysics* **7**(4): 796–803.

Stearns, L. and Hamilton, G. (2005). A new velocity map for Byrd Glacier, East Antarctica, from sequential ASTER satellite imagery, *Annals of Glaciology* **41**: 71–76.

Thompson, R. D. and Kells, B. R. (1973). Mass balance studies on the Whakapapanui Glacier, *Technical Report 107*, New Zealand International Association fo Hydrological Science Publication.

Tomlinson, A. I. (1992). Precipitation and the atmosphere, *in* M. P. Mosley (ed.), *Waters of New Zealand*, New Zealand Hydrological Society.

Ulaby, F. T., Moore, R. K. and Fung, A. K. (1986). *Microwave Remote Sensing: Active and Passive Volume III: From Theory to Applications*, Artech House, Norwood.

Van Looy, J., Forster, R. and Ford, A. (2006). Accelerating thinning of Kenai Peninsula glaciers, Alaska, *Geophysical Research Letters* **33**: L21307.

Vignon, F., Arnaud, Y. and Kaser, G. (2003). Quantification of glacier volume change using topographic and ASTER DEMs, *Geoscience and Remote Sensing Symposium*, Vol. 4, IGARSS '03 Proceedings, IEEE International, pp. 2605–2607.

Watson, M. I. (1995). *Geophysical and Glaciological Studies of the Tasman and Mueller Glaciers*, Unpublished masters thesis, University of Auckland.

Yamaguchi, Y., Kahle, A. B., Tsu, H., Kawakami, T. and Pniel, M. (1998). Overview of Advanced Spaceborne Thermal Emission and Reflection Radiometer (ASTER), *IEEE Transactions on Geoscience and Remote Sensing* **36**(4): 1062–1071.